Mul1/Mfn2-mediated mitochondrial dynamics and bioenergy support protective effects of ginsenoside CK against cerebral ischemia/reperfusion injury

Running title: Inhibition of Mul1-mediated Mfn2 ubiquitination against cerebral I/R injury

Qingxia Huang[a,b], Jing Li[b], Jinjin Chen[b], Zepeng Zhang[a,b], Peng Xu[c], Hongyu Qi[b], Zhaoqiang Chen[b], Jiaqi Liu[b], Jing Lu[a,b], Mengqi Shi[d], Yibin Zhang[c], Ying Ma[c], Daqing Zhao[b*], Xiangyan Li[b*]

[a] Research Center of Traditional Chinese Medicine, College of Traditional Chinese Medicine, Changchun University of Chinese Medicine, Changchun, Jilin, China

[b] Jilin Ginseng Academy, Key Laboratory of Active Substances and Biological Mechanisms of Ginseng Efficacy, Ministry of Education, Jilin Provincial Key Laboratory of Bio-Macromolecules of Chinese Medicine, Changchun University of Chinese Medicine, Changchun, Jilin, China

[c] Department of Encephalopathy, College of Traditional Chinese Medicine, Changchun University of Chinese Medicine, Changchun, Jilin, China

[d] Department of Graduate Administration, College of Traditional Chinese Medicine, Changchun University of Chinese Medicine, Changchun, Jilin, China

*__Corresponding authors:__ Daqing Zhao, Xiangyan Li, Jilin Ginseng Academy, Key Laboratory of Active Substances and Biological Mechanisms of Ginseng Efficacy, Ministry of Education, Jilin Provincial Key Laboratory of BioMacromolecules of Chinese Medicine, Changchun University of Chinese Medicine, Changchun, Jilin, China. Tel.: +86-431-86177630, Fax: +86-431-86177630. Email: zhaodaqing1963@163. com; xiangyan_li1981@163.com.

Word count: 3994

Data availability: The data that support the findings of this study are available from the corresponding author upon reasonable request.

Funding statement: This work was supported by the National Key Research and Development Program of China (2017YFC1702103) to Xiangyan Li, National Natural Science Foundation of China (U19A2013) to Daqing Zhao, and the Science and Technology Development Plan Project of Jilin Province (20190101010JH, 202002053JC) to Xiangyan Li, and Jilin Provincial Administration of Traditional Chinese Medicine (2020168) to Qingxia Huang.

Author contributions statement: DZ, XL and QH conceived and designed this study; QH and JLi participated in the study design and interpreted data; JC and ZZ prepared the draft manuscript; HQ and ZC participated in the data collection and analysis; JQL, PX and JLu performed the histological and immunobiological experiments and behavioral experiments; QH, MS, YM and YZ contributed to writing and revising the manuscript. All authors have read and approved final manuscript.

Conflict of interest statement: All authors agree to submit this article and declare no conflict of interest

Ethics approval statement: All animal care and experimental procedures were approved by the Animal Ethics Committee of Changchun University of Chinese Medicine (Changchun, China, approval No. 2021121)

Declaration of transparency and scientific rigour: This declaration acknowledges that this paper adheres to the principles for transparent reporting and scientific rigour of preclinical research as stated in the BJP guidelines for Design & Analysis, Immunoblotting and Immunochemistry, and Animal Experimentation, and as recommended by funding agencies, publishers and other organizations engaged with supporting research.

All authors have read and have abided by the statement of ethical standards for manuscripts submitted to *British Journal of Pharmacology*.

This paper is our unpublished work and has not been submitted to any other journal for review.

Abbreviations:

I/R, ischemia/reperfusion; CK, compound K; RET, reverse electron transport; OXPHOS, oxidative phosphorylation; Mul1, mitochondrial E3 ubiquitin ligase 1; OPA1, optic atrophy protein 1; DRP1, dynamin-related protein 1; FIS1, fission 1 protein; MCAO, middle cerebral artery occlusion; PI3K, phosphatidylinositol 3-kinase; AMPK, AMP-activated protein kinase; OGD, oxygen glucose deprivation; CA, carotid artery; ECA, external carotid artery; ICA, internal carotid artery; Mfn2, mitofusin2; FCCP, carbonyl cyanide 4-(trifluoromethoxy) phenylhydrazone; OCR, oxygen consumption rate; ECAR, extracellular acidification rate; Glu, glucose; Olig, oligomycin; 2-DG, 2-D-glucose; Rot, rotenone; AA, antimycin A; TTC, 2,3,5-triphenyltetrazolium chloride; TEM, transmission electron microscopy; OGD/R, oxygen glucose deprivation/reperfusion; ETC, electron transport chain; mito-ROS, mitochondrial ROS.

Bullet point summary

What is already known

- Mitochondrial fission-fusion dynamics and bioenergy dysfunctions are participated in cerebral ischemia/reperfusion (I/R) injury.
- Ginsenoside CK protects against cerebral I/R-induced ischemic stroke.

What this study adds

- I/R injury upregulates the binding of Mul1 and Mfn2 to enhance dynamic and bioenergy dysfunction.
- Mul1/Mfn2-mediated dynamic and bioenergy is involved in the beneficial effect of ginsenoside CK against cerebral I/R injury.

What is the clinical significance

- Mul1-mediated Mfn2 ubiquitination may be a promising and effective target against ischemic stroke.
- Ginsenoside CK may be a potential drug for targeting the Mul1/Mfn2 ubiquitination against I/R injury.

Abstract

Background and Purpose: Mitochondrial fission-fusion dynamics and bioenergy dysfunctions are participated in cerebral ischemia/reperfusion (I/R) injury. Our study aims to investigate the role of Mul1-dependent Mfn2 ubiquitination and its mediated mitochondrial dysfunctions and explain the molecular mechanism of ginsenoside compound K (CK) targeting Mul1 against cerebral I/R injury.

Experimental Approach: We used a combination of *in vitro* and *in vivo* models, including oxygen and glucose deprivation/reperfusion-induced PC12 cell model and middle cerebral artery occlusion/reperfusion-induced rat model, to mimic I/R injury. The potential mechanisms and pharmacological effects of ginsenoside CK on mitochondrial dynamics and bioenergy were evaluated by Mul1 knockdown and pharmacological antagonism study using a series of experiments.

Key Results: I/R injury stimuli upregulated the binding of Mul1 with Mfn2 to regulate Mfn2 ubiquitination and degradation, which resulted in increased mitochondrial fission, bioenergy dysfunction, neuronal apoptosis, and neurological impairment. Knockdown of Mul1 exerted beneficial effect on cerebral I/R-induced neuronal death by abolishing mitochondrial fission, mitophagy, and bioenergy dysfunction. More importantly, ginsenoside CK mainly inhibited Mul1 expression to reduce Mfn2 ubiquitination and mitochondrial translocation of DRP1, thereby inhibiting mitochondrial fission, mitophagy and mitochondrial apoptosis against cerebral I/R injury in both *in vitro* and *in vivo* models.

Conclusions and Implications: These data for the first time explain molecular basis of the Mul-dependent mitochondrial dysfunctions during I/R damages and provide the evidence that ginsenoside CK may be a promising therapeutic agent against cerebral I/R injury by targeting Mul1/Mfn2-mediated mitochondrial dynamics and bioenergy.

Keywords: Cerebral ischemia/reperfusion injury; mitochondrial dynamic; bioenergy; ginsenoside compound K; Mul1/Mfn2 ubiquitination

1 INTRODUCTION

Cerebral ischemia/reperfusion (I/R) injury is a pathological condition characterized by the recovery of blood circulation in the treatment of ischemic stroke, which eventually leads to acute neurological deficit (Han et al., 2017). A growing body of preclinical and clinical evidence indicate that mitochondria as dynamic organelles manage to retain the balance of dynamic fusion/fission in neuron I/R situations (Liu et al., 2018). Mitochondrial fusion accelerates the exchange of nutrition materials and assists in the repair of damaged mitochondria, meanwhile mitochondrial fission occupy an important position for the removal of defective mitochondria through mitophagy (Gao & Hu, 2021; Kumar et al., 2016). During I/R injury, the superoxide production by complex I reverse electron transport (RET) results in stunted mitochondrial fusion and fission, in conjunction with traumatic mitophagy, leads to the dysfunctions of Krebs cycle and oxidative phosphorylation (OXPHOS) (Ten & Galkin, 2019). Abnormal mitochondrial bioenergy leads to reduce mitochondrial respiration function and neuronal injury (Chipuk et al., 2021). Hence, dynamic regulation (elevated fusion and suppressed fission) and bioenergy promotion of mitochondria may play neuroprotective effects against cerebral I/R-induced injury.

Mitochondrial E3 ubiquitin ligase 1 (Mul1) is a multifunctional mitochondrial membrane protein and acts as the first-line surveillance of mitochondrial dynamics and energy supply in neuronal I/R injury (Guo et al., 2019; Liu & Dong, 2020). In neurons, mitochondrial dynamic fusion is mainly controlled by optic atrophy protein 1 (OPA1) and mitofusins (Mfn1 and Mfn2), while fission depends on dynamin-related protein 1 (DRP1) and fission 1 protein (FIS1) (Burté et al., 2015; Schmitt et al., 2018). In mammalian systems, E3-active, C-terminal RING finger domain of Mul1 faces the cytosol, which can stabilize DRP1 and degrade mitofusins through ubiquitin-like modifier and ubiquitination (Igarashi et al., 2020; Yuan et al., 2019). As expected from Mul1 protein with these proposed biochemical activities, I/R-induced Mul1 overexpression in neurons results in smaller and more fragmented mitochondria, accompanying by enhancing mitophagy, inhibited OXPHOS, energy homeostasis imbalance, and mitochondrial apoptosis (Puri et al., 2020). Thus, the suppression of

Mul1 activity and expression can regulate mitochondrial dynamics, mitophagy to enhance mitochondrial bioenergy against I/R damage in neurons.

Ginsenoside compound K (CK), one of main active metabolites from a traditional Chinese medicine, *Panax ginseng*, has a good safety and bioavailability in clinical trials, and exerts neuroprotective effects in neurodegenerative diseases and cerebral ischemic stroke (Huang et al., 2020; Oh et al., 2020; Oh & Kim, 2016; Sharma & Lee, 2020). One research have revealed that ginsenoside CK reduced the infarct volume of cerebral I/R model induced by middle cerebral artery occlusion (MCAO) and suppressed microglial activation in the mice ischemic cortex (Park et al., 2012). In addition, our previous studies have demonstrated that ginsenoside CK inhibited autophagy-mediated apoptosis against I/R injury through regulation of phosphatidylinositol 3-kinase (PI3K) and AMP-activated protein kinase (AMPK) pathways (Huang et al., 2020). Our literature review have found that ginsenoside CK can target mitochondrial function to inhibit metabolic stress (Huang, Gao, et al., 2021). Importantly, our latest *in vivo* and *in vitro* studies have shown that ginsenoside Rc, a key metabolic precursor of ginsenoside CK can inhibit brain I/R injury by increasing mitochondrial biosynthesis and ATP production, and inhibiting mitochondrial apoptosis (Huang, Su, et al., 2021). The studies above indicate that ginsenoside CK can significantly reduce cerebral I/R injury, and its effect may be related to mitochondrial function and energy metabolism. However, the underlying protective mechanism that ginsenoside CK regulates mitochondrial fusion/fission and bioenergy production against I/R damage remains to be elucidated. Hence, the present study was designed to investigate the pharmacological mechanism of ginsenoside CK against cerebral I/R-induced injury based on Mul1-mediated mitochondrial dynamics and bioenergy in *in vitro* and *in vivo* study.

2 METHODS

2.1 Cell culture and oxygen glucose deprived/reperfusion (OGD/R) model

PC12 cells were purchased from the American Type culture Collection (ATCC, Manassas, VA, USA) and cultured in high-glucose DMEM medium supplemented with 7.5% fetal bovine serum, 2.5% horse serum, and 100 U/mL penicillin/streptomycin at 37°C in a humidified 5% CO_2 atmosphere. As previously reported, oxygen glucose deprived (OGD) incubation was carried out using an enclosed BioSpa automated incubator (BioTek, Winooski, VT, USA) flushed with N_2 (95%) and CO_2 (5%) for 2 h. Then, the medium was changed to the normal incubation to 12 h for reperfusion (Huang et al., 2020; Huang, Su, et al., 2021). The ginsenoside CK treatment group was incubated with ginsenoside CK for 48 h before OGD/R modeling.

2.2 Animals and middle cerebral artery occlusion model

All animal experiments were carried out in compliance with institutional guidelines and were approved by the Animal Ethics Committee of Changchun University of Chinese Medicine (Changchun, China, approval No. 2021121). Animal studies strictly adhered to the ARRIVE guidelines and the recommendation made by the British Journal of Pharmacology (Lilley et al., 2020). Male SD rat (180−200g) were supplied by the Animal Core Facility of Changchun Yisi Experimental Animal Technology Co. Ltd (Changchun, China). Rats were housed in an environmentally controlled room and accessed to standard rodent chow and tap water ad libitum.

The rats were assigned to three groups (sham, I/R, and I/R+CK groups) followed by the CK pretreatment and model establishment with ten animals at least per group. The rats in sham and I/R groups ($n \geqslant 10$, each group) were received double-distilled water (ddH_2O, 500μl) and the rats in I/R+CK group ($n \geqslant 10$) were administered orally with ginsenoside CK (10 mg/kg/day, 500μl, dissolved in ddH_2O) were for 14 days prior to model establishment. During the procedure of I/R model, the rats were anaesthetized by injection of 10% chloral hydrate (400 $mg \cdot kg^{-1}$, i.p.) and maintained under anesthesia with 1-1.5% isoflurane inhalation in air by an animal anaesthesia

ventilator system (RWD Life science, Shenzhen, China). All efforts were taken to minimize the number of animals used and minimal suffering. The focal cerebral ischemia in the rats of I/R and I/R+CK groups was induced by MCAO model, as the previous studies (Bederson et al., 1986; Kim et al., 2020). After the induction of anesthesia and disinfected, the carotid artery (CA) was exposed to isolate the external carotid artery (ECA) and the internal carotid artery (ICA). A small hole in ECA was cut and a length of 6 mm nylon monofilament was inserted into the left ICA. The wound of the rat was closed and kept for 1 h in a heated cage after occlusion. After occlusion for 1 h, reperfusion was administered through the withdrawal filament. Finally, the skin was sutured surgically. In the sham group, an identical surgical procedure was performed without insert the nylon monofilament. After I/R surgery, the rats were sacrificed after anesthetization by 10% chloral hydrate by which to ensure minimal discomfort.

2.3 Antibodies and reagents

Oligomycin B (ab143424), antimycin A (ab141904) and antibodies against total OXPHOS (ab110413), Mfn1 (ab104274), Mfn2 (ab56889), DRP1 (ab56788), ubiquitin (Abcam, ab140601), FIS1 (ab71498), and OPA1 (ab90857) were obtained from Abcam (Cambridge, MA, USA). Antibodies to TOM20 (#42406), LC3A/B (#4108), P-DRP1 (Ser637, #4867), and β-Actin (#3700) were purchased from Cell Signaling Technology (Beverly, MA, USA). Mul1 (16133-1-AP) and Parkin (14060-1-AP) antibodies were purchased form Proteintech (Wuhan, Hubei, China). Carbonyl cyanide 4-(trifluoromethoxy) phenylhydrazone (FCCP, C2920), rotenone (R8875), and Mdivi-1 (M0199) were purchased from Sigma-Aldrich (St. Louis, MO, USA).

2.4 siRNA transfection

Pre-designed siRNA for rat Mul1 (siG150514163245-1-5) and negative control siRNA (siB160812022401-1-5) were provide by the RiboBio (Guangzhou, China) and transfected into PC12 cells using Lipofectamine RNAiMAX (Invitrogen). Briefly, the

dilute siRNA and transfection reagent in Opti-MEM (Invitrogen) were incubation for 5 min at room temperature to allow the formation of siRNA-lipid complexes. After washing twice by Opti-MEM, the cells were incubated with the siRNA-lipid complexes for 48 h and examined the efficiency of siRNA silencing by Western blot, and then subjected to various treatments as planned (Cheng et al., 2020).

2.5 Mitochondria isolation

Mitochondrial part were prepared from PC12 cells or brain tissues using a mitochondria isolation kit (C3606, Beyotime Institute of Biotechnology, Ltd., Shanghai, China), as following manufacturer's recommendation (Yu et al., 2016). Briefly, cells and tissues were mechanically disrupted by homogenizer in isolation reagent containing phenylmethylsulfonyl fluoride. The cell debris and nuclei were removed from mitochondria fractions by centrifugation at 1,000 g for 10 min. The samples were subject to another round of centrifugation at 11,000 g for 10 min to obtain highly enriched mitochondrial fractions, and the supernatant was the cytoplasmic protein, the pellet was used as isolated mitochondrial fractions.

2.6 Co-Immunoprecipitation (co-IP)

Proteins from PC12 cells and brain tissues were extracted in NP-40 lysis buffer (Beyotime) contained with a complete protease inhibitor cocktail (Sigma-Aldrich) (Zhang et al., 2019). Protein extracts were subjected to centrifugation at 12,000 g for 12 min. After the specified antibodies were bound to protein lysate at 4 °C overnight, the antigen-antibody complex was immunoprecipitated with the A/G magnetic beads at room temperature for 1 h. After separating the beads with a magnetic rack, the pellets were eluted with sample buffer and boiled at 100 °C for 5 min. Magnetic beads were separated, supernatant was loaded onto an acrylamide gel.

2.7 Mitochondrial and mitophagy morphology

To visualize mitochondria and lysosomes, neurons were stained with 50 nM of MitoTracker Green Reagent (Invitrogen) or Lyso-Tracker Red (Beyotime) for 40 min

at 37°C followed by addition of Hoechst 33342 (Invitrogen) as the manufacturer's instructions. The 20-30 mitochondria or lysosomes per cell were measured using the C2 confocal microscope with the ZEN analysis software (Nikon, Japan). Mitochondrial aspect ratio is used to evaluate mitochondrial fragment, and a smaller aspect ratio indicates a higher degree of fission and fragment. The co-localization of mitochondrial and lysosomal signals was used to evaluate the level of mitophagy (Puri et al., 2019).

2.8 Seahorse analysis

To investigate the ATP production from OXPHOS and glycolysis, oxygen consumption rate (OCR) and extracellular acidification rate (ECAR) were determined using the Seahorse XFe24 analyzer (Seahorse Bioscience, Billerica, MA, USA) as reported previously (Huang, Su, et al., 2021). Briefly, the cells were plated in Seahorse XFe24 cell culture plate before pretreatment with ginsenoside CK and/or OGD/R incubation. The media was then exchanged with Seahorse XF DMEM media (Seahorse Bioscience) contained with 2 mM glutaMAX (Invitrogen), 1 mM sodium pyruvate (Invitrogen), and 10 mM glucose, which were equilibrated for 30 min at 37°C before the experiment. Cellular ATP, OCR or ECAR was monitored in basal condition (before any addition) and after addition of glucose (Glu), oligomycin (Olig), 2-D-glucose (2-DG), FCCP or rotenone (Rot) & antimycin A (AA) with three cycles of mixing (150 sec), waiting (120 sec) and measuring (210 sec).

2.9 2,3,5-triphenyltetrazolium chloride (TTC) staining

Twenty-four hours after reperfusion, the rat brains were stripped and coronally sliced at 2.0-mm intervals from the frontal poles as previously described (Gong et al., 2021). Then the sections were immersed in 0.25% TTC solution at 37°C for 30 min. The area of infarct of serial sections was quantified with Image J by an investigator blinded to the experimental groups. The degree of infarction was calculated using the following calculation formula: infarct ratio (%) = infarct volume (mm^3)/total coronal section (mm^3) × 100%.

2.10 Neurological deficit score

The evaluation of a neurological deficit at 12 h or 24 h of reperfusion was based on the method described by Longa et al (Longa et al., 1989). Score 0 point: no observable deficits; score 1 point: mild circling movements when picked up by a mouse tail and attempts to rotate to the contralateral side; score 2 point: consistent strong and immediate circling or an animal only turned to the surgery contralateral side while the animal was suspended by holding the tail; score 3 point: severe rotation progressing into loss of walking or righting reflex; score 4 point: an animal did not walk spontaneously and had some degree of consciousness.

2.11 Transmission electron microscopy (TEM)

After pretreatment with ginsenoside CK and/or I/R injury, brain tissue was cut at 2-mm sections to fix in ice-cold 2.5% glutaraldehyde solution for 15 min. Then, tissue sections were post-fixed in 0.7% potassium ferrocyanide, stained with 2.5% uranyl acetate in 0.1 M maleate, and embedded in Eponate (TedPella, CA, USA). Tissue sections were polymerized overnight and immersed in liquid nitrogen. Thin sections with 60-80 nm were cut with a diamond knife on a Leica EM UC7 ultramicrotome with ultra 45° (Daitome) and collected onto copper grids, which were stained with 4% uranyl acetate in 50% methanol and 5% citrate (Geng et al., 2019). Images were captured with transmission electron microscope (TECNAI G2 20 TWIN, FEI, Hillsboro, OR, USA).

2.12 Data and statistical analysis.

All the *in vivo* and *in vitro* experimental groups were designed to establish equal size, blinding and randomization, and the data and statistical analysis of this study complies with the recommendations of the British Journal of Pharmacology on experimental design and analysis in pharmacology (Lilley et al., 2020). All group sizes represent the numbers of experimental independent values, and these independent values were used to evaluate statistical analyses, and statistical analyses were undertaken only for experiments where each group sizes (n) $\geq$ 5. Values are

expressed as mean ± SD in *in vitro* study and mean ± SEM in *in vivo* study. The two-tailed Student's t-test were used to calculate the comparison for two groups. Multigroup studies comparisons were performed using the One-way ANOVA followed by a Tukey's post hoc test. The post hoc tests were conducted only if the F in ANOVA achieved the necessary statistical significance level and there was no significant variance inhomogeneity. The analyses were performed by GraphPad Prism 8.0. $P < 0.05$ was considered statistically significant (Raimundo et al., 2021).

3 RESULTS

3.1 Mul1 binds to Mfn2 and negatively regulates its level through ubiquitination in OGD/R and I/R-induced injury models

In order to study which regulators of mitochondrial dynamics are mainly regulated by Mul1 in I/R injury, we first detected the protein expression of known regulators of mitochondrial dynamics in PC12 cells transfected with si-Mul1 or si-Ctrl siRNAs. As shown in Fig. 1A-1B and Fig. S1A, we noted that OGD/R incubation led to the elevated expressions of Mul1, DRP1 and FIS1 involved in mitochondria fission and the decreased levels of Mfn1, Mfn2, P-DRP1 (S637), and OPA1 related to mitochondrial fusion in the mitochondria of PC12 cells. Importantly, only DRP1 and Mfn2 protein levels were abolished in si-Mul1-transfected PC12 cells in response to OGD/R incubation, compared to si-Ctrl group. Next, we determined if Mul1 and Mfn2 interact physically, and if Mul1 regulates Mfn2 level through ubiquitination. In the cerebral ischemic penumbra of rat model (Fig. 1C), we observed that the expression of ubiquitinated protein was increased significantly after I/R incubation, compared to Sham group (Fig. 1SB). In addition, co-IP experiments demonstrated that the interaction of Mul1 and Mfn2 and the ubiquitination level of Mfn2 were significantly increased in I/R group (Fig. 1D). Consistent with PC12 cells subjected to OGD/R incubation, the translocation of DRP1 from the cytoplasm to the mitochondria was increased significantly in I/R group (Fig. 1E- Fig. 1F). Collectively, *in vitro* and *in vivo* experiments demonstrated that OGD/R incubation or I/R injury causes the increase of Mul1expression, which increases the ubiquitination of Mfn2 and the

translocation of DRP1 to the mitochondria.

3.2 Mul1 mediates neuronal mitochondria dynamic and bioenergy variations in OGD/R and I/-induced injury models.

Mitochondria dynamics and bioenergy play critical roles to maintain the mitochondrial population and function (Chandel, 2014). In agreement with a previous report, we found that OGD/R incubation significantly reduced the mitochondrial aspect ratio, which means that mitochondrial fission is elevated and fusion is reduced in PC12 cells (Fig. 2A). However, mitochondrial division was significantly reduced after OGD/R incubation in the Mul1-knockdown PC12 cells, compared with si-Ctrl transfected group (Fig. 2A). To further monitor mitophagy, we fluorescently labeled in living cells, and found that the co-localization of lysosomes and mitochondria was increased significantly by OGD/R incubation in the si-Ctrl group, while in the Mul1 knockdown group, OGD/R-induced the co-localization of mitochondrial and lysosomal signals were significantly reduced (Fig. 2B and Fig. S2A-Fig. S2B). Parkin functions as an E3 ubiquitin ligase and translocates from the cytosol to mitochondria to promote mitochondria degradation by mitophagy. A similar increase in Parkin and TOM20 co-localization, a mitophagy marker was observed in rat brain tissues subjected to I/R damage (Fig. 2C). We then determined whether mitochondrial bioenergy in OGD/R-induced injury is dependent on Mul1. As expected, Mul1 silencing by siRNA blocked the decreases of ATP amount induced by OGD/R (Fig. 3A). Seahorse analysis showed that Mul1 silencing recovered multiple parameters of mitochondrial respiration, including basal respiration (Basal), maximal respiration capacity (MRC), spare respiration capacity (SRC), and ATP-linked respiration (ATP) induced by OGD/R, compared with si-Ctrl transfected group ((Fig. 3B-3C and Fig, S3A). Western blot analysis showed that OGD/R-induced decreases of complex I-V levels were abolished by si-Mul1 siRNAs, compared to the si-Ctrl transfected group (Fig. 3D and Fig. S3B). Given that mitochondrial dynamics and bioenergy are important for maintaining cell survival, we thus investigated whether knockdown of Mul1 exerted inhibitory effect on mitochondrial apoptosis. Notably, OGD/R

incubation led to mitochondrial membrane potential reduction and mitochondrial apoptosis with increased cyto C and reduced Bcl-2/Bax, which were abolished by Mul1 silencing (Fig. 3E-3F and Fig. S3C-S3D). Taken together, these data indicate that Mul1 regulates mitochondrial dynamics and bioenergy, which is a critical factor in OGD/R and I/R injury.

3.3 Ginsenoside CK rescued OGD/R-induced mitochondrial dysfunctions depending on Mul1 inactivation

Our previous studies have shown that ginsenoside CK can significantly inhibit OGD/R-induced mitochondrial damage and apoptosis in neurons and cardiomyocytes (Huang et al., 2020; Li et al., 2018). Therefore, we further analyzed whether ginsenoside CK targets Mul1 to restore mitochondrial function. Firstly, the dose-dependent effect of ginsenoside CK on ATP content was evaluated by a luminescence assay. Our results showed that ginsenoside CK at the concertation of 2, 4, and 8 μM significantly restored the decrease in ATP synthesis caused by OGD/R (Fig. S4A). At the same time, it found that ginsenoside CK increased the ATP content mainly from mitochondria, which had no obvious effect on ATP production from glycolysis (Fig. 4A). To further verify the origin of increased ATP mediated by ginsenoside CK, OCR was monitored in real time to measure the key parameters of mitochondrial function by adding different modulators of respiration. As expected, we found that ginsenoside CK caused an enhancement in ATP production and respiratory capacity, but had no significant effect on ECAR, glycolytic capacity and reserve in the OGD/R-induced injury (Fig. 4B-Fig. 4C). To evaluate the effect of ginsenoside CK on the electron transport chain (ETC), we examined the expressions and activities of the mitochondrial complex I-V. As shown in Fig. 4D-4E and Fig. S4B, the results showed that ginsenoside CK had no obvious recovery effect on the reduction in the levels of complex II-V, but it had a significant promotion effect on the activities of mitochondrial complex I (NADH-CoQ reductase) and III (CoQ-Cytochrome C reductase). Importantly, we found that the effect of ginsenoside CK pretreatment in promoting mitochondrial oxygen consumption in OGD/R-injured PC12 cells was

completely abolished by Mul1 knockdown (Fig. 4F and Fig. S4C), compared to the si-Ctrl group. The results above suggest that ginsenoside CK rescues OGD/R-induced mitochondrial dysfunction, which might be dependent on Mul1 signaling.

3.4 Ginsenoside CK balance mitochondria dynamic and mitophagy are Mul1 dependent in OGD/R-induced PC12 model

We further evaluated the effect of ginsenoside CK on mitochondrial dynamics and mitophagy in OGD/R injury and whether it is Mul1-dependent. As shown in Fig. S5A-Fig. S5B, ginsenoside CK incubation decreased mitochondrial fragmentation in a dose-dependent manner, compared with the OGD/R group. Consistent with expectation, knockdown of Mul1 blocked the inhibitory effect of ginsenoside CK on mitochondrial fission in OGD/R-injured PC12 cells (Fig. 5A). To determine whether Mul1-regulated mitophagy contributes to neuroprotection of ginsenoside CK against OGD/R injury, Parkin translocation to mitochondria and co-localization of mitochondria and lysosomes were evaluated in si-Ctrl or si-Mul1 transfected cells. The Parkin translocation to mitochondria induced by OGD/R significantly was reversed by ginsenoside CK, while Mul1 knockdown markedly abrogated the mitigated effect of ginsenoside CK in terms of mitophagy (Fig. 5B and Fig. S5C). Similarly, Mul1 knockdown counteracted the effect of ginsenoside CK in reducing the co-localization of mitochondria and lysosomes (Fig. 5C and Fig. S5D). The results above indicate that the effects of ginsenoside CK on mitochondrial dynamics and mitophagy are mediated by the Mul1 signaling in OGD/R-induced PC12 cell injury model.

3.5 Ginsenoside CK inhibits OGD/R-induced neuronal injury by regulating the Mul1-Mfn2 pathway in a mitochondrial dynamic-dependent manner

To further clarify the regulatory effect of ginsenoside CK on Mul1 and mitochondrial dynamics-related signaling pathways during OGD/R injury, we separated cytoplasmic and mitochondrial proteins of PC12 cells untreated or treated with ginsenoside CK for Western blot analysis. OGD/R incubation caused the

decreased DRP1 phosphorylation at S637 and the slightly increased DRP1 in the cytoplasmic and mitochondrial proteins (Fig. 6A and Fig. S6A). Meanwhile, we observed that OGD/R incubation resulted in the significant decreases of mitochondrial fusion-related proteins, and the obvious increases of Mul1 and mitochondrial fission-related proteins (Fig. 6A and Fig. S6A). Importantly, our results showed that ginsenoside CK pretreatment prior to OGD/R incubation significantly reduced the expression of Mul1 and the translocation of DRP1 to mitochondria, as well as increased Mfn2 expression in mitochondria (Fig. 6A and Fig. S6A). Since Mul1 mainly regulates mitochondrial dynamics through ubiquitination of Mfn2, we then conducted a co-IP experiment to verify the regulatory effect of ginsenoside CK on the Mul1-Mfn2 signaling pathway. As expected, when Mul1 was immunoprecipitated, the protein binding of Mfn2 with Mul1 was significantly reduced after ginsenoside CK treatment, which means that ginsenoside CK reduced the degradation of Mfn2 by Mul1 after OGD/R incubation (Fig. 6B). In contrast, after Mfn2 was immunoprecipitated, OGD/R-induced Mul1 expression and the level of ubiquitination were obviously reduced by ginsenoside CK, which suggests that ginsenoside CK pretreatment did reduce Mul1-mediated Mfn2 ubiquitination and degradation by during the OGD/R injury (Fig. 6B). To identify the contribution of ginsenoside CK firstly regulates the binding of Mul1 and Mfn2, and then influences mitochondrial fission, mitophagy and mitochondrial apoptosis, Mdivi-1, a widely used inhibitor of mitochondrial fission, was introduced to investigate the mechanism of ginsenoside CK in OGD/R-induced injury. Combination with Mdivi-1 treatment, the effect of ginsenoside CK in reducing Mul1 expression and increasing Mfn2 expression was significantly abolished, while the effect of inhibiting the translocation of DRP1 into mitochondria was preserved (Fig. 6C and Fig. S6B). In addition, Mdivi-1 treatment also counteracts the phenomenon that ginsenoside CK inhibited Parkin translocation to mitochondria (Fig. 6D and Fig. S6C) and the production of mitochondrial ROS to prevent OGD/R injury (mito-ROS, Fig. 6E and Fig. S6D). These results suggest that ginsenoside CK mainly targets Mul1 to reduce the ubiquitination and degradation of Mfn2, resulting in increased Mfn2 expression to inhibit mitochondrial fission,

mitophagy and mitochondrial apoptosis in OGD/R neuronal injury.

3.6 Ginsenoside CK counteracts I/R-induced neurological impairment and mitochondrial dysfunction in rats

Cerebral I/R causes exacerbated neuronal damage involving mitochondrial dysfunction (Kalogeris et al., 2014). To investigate the therapeutic effect of ginsenoside CK on cerebral I/R injury, we evaluated the infarct volume, neurological deficit score, and brain water content in a rat model after 12 h or 24 h reperfusion. TTC staining showed that the infarct volume of the ginsenoside CK pretreatment group was significantly smaller than that of I/R group (Fig. 7A-7B). After ginsenoside CK pretreatment, the neurological function score was decreased significantly, compared to I/R group (Fig. 7C). Moreover, ginsenoside CK pretreatment can also relieve cerebral edema caused by I/R injury (Fig. 7D). In addition, H&E and Nissl staining showed that the neurons in cortex, CA1, CA3, striatum, and gyrus in rats with cerebral I/R injury were arranged loosely, and exhibited cell body shrinkage, partial nuclear fragmentation, nuclear pyknosis, nucleolar blurring, and even degeneration (Fig. 7E and Fig. S7A-S7B). Compared to I/R injury group, ginsenoside CK administration significantly restored the damages of neurons in the cerebral cortex and CA1 regions (Fig. 7E). Detection of a neuron marker, MAP2 by immunofluorescence staining also verified the neuroprotective effect of ginsenoside CK pretreatment (Fig. 7F-Fig. 7G). To further confirm the inhibitory effect of ginsenoside CK on I/R-induced mitochondrial dysfunction, we extracted mitochondria from fresh brain tissues for determining oxygen consumption and mitochondrial complex enzyme activity. As shown in Fig. 7H and Fig. 7I, ginsenoside CK pretreatment significantly restores the reductions of maximal respiration capacity (no effect on basal respiration) and the activities of complex I and III induced by I/R. As *in vitro* experiments, ginsenoside CK has no effect on the protein expression of mitochondrial complex in the I/R-injured rat model (Fig. S7C- Fig. S7D). Together, the results above verified the effect of ginsenoside CK on the inhibition of neuronal damage and bioenergy imbalance in the *in vivo* I/R model.

3.7 Ginsenoside CK reduces mitochondrial fission and mitophagy in rat I/R model

We further verify the regulatory role of ginsenoside CK on mitochondrial dynamics and mitophagy in rat I/R model. First, we observed the ultrastructure of mitochondria through TEM and analyzed the mitochondrial aspect ratio, the number of mitochondria and autophagosomes. As shown in Fig. 8A, ginsenoside CK pretreatment significantly reduced mitochondrial division and mitophagy, and slightly increases the mitochondria account, compared to I/R model group. Moreover, we observed the expressions of LC3, Parkin, and TOM20 in the different areas of brain tissue using a laser confocal microscope and performed the colocalization analysis. In the CA1 region of brain tissue, the increase in LC3 expression after I/R incubation was significantly offset by ginsenoside CK pretreatment, while this phenomenon was not observed in the CA3 region (Fig. 8B and Fig. S8A-Fig. S8C). Interestingly, we found that ginsenoside CK pretreatment could significantly inhibit the increase of Parkin-TOM20 colocalization induced by I/R in the all regions of rat brain tissues, including cortex, gyrus, CA1 and CA3 regions (Fig. 8C-8D). Together, these *in vivo* results demonstrate that ginsenoside CK administration significantly reduces I/R-induced mitochondrial fission and mitophagy in brain tissue.

3.8 Ginsenoside CK inhibits the ubiquitination of Mfn2 and the translocation of DRP1 by regulating Mul1 in I/ R rat model

By immunoblot analyses, we found that ginsenoside CK pretreatment significantly abolished I/R-induced increased Mul1 expression, DRP1 translocation, and reduced Mfn2 expression, especially in mitochondria, similar to *in vitro* experiments results (Fig. 9A and Fig. S9A). Confocal imaging further revealed that the reduction in Mfn2 expression induced by I/R was inhibited by ginsenoside CK pretreatment in the cortex and CA1 regions of brain tissue (Fig. 9B and Fig. S9B-S9C). Importantly, ginsenoside CK pretreatment augmented Mfn2 expression, accompanied by a significant reduction in ubiquitinated protein expression after I/R processing (Fig. 9C and Fig. S9D). To verify whether ginsenoside CK pretreatment directly reduces the effect of Mul1-mediated the ubiquitination of Mfn2, we then

analyzed the interaction of Mul1 and Mfn2 by co-IP experiment. Indeed, after Mul1 was immunoprecipitated, ginsenoside CK significantly blunted the binding of Mul1 to Mfn2 in cortex tissues during I/R (Fig. 9D). Similarly, the binding of Mfn2 to Mul1 was also inhibited by ginsenoside CK pretreatment, when Mfn2 was immunoprecipitated. Importantly, the ubiquitination of Mfn2 was significantly inhibited in the CK group, compared to that of I/R group (Fig. 9D). Collectively, these data confirmed that ginsenoside CK pretreatment reduces the binding affinity of Mul1 and Mfn2 to inhibit the ubiquitination and degradation of Mfn2, thereby elevating the protein level of Mfn2 and attenuating mitochondrial translocation of DRP1 against I/R injury.

4 DISCUSSIONS

Neurons, as a postmitotic and high-energy-demand cell, are inevitably to be more prone to mitochondrial pathologies (Iwata et al., 2020). Preventing mitochondrial dysfunction during cerebral IR injury remains a potential and promising treatment strategy (Liu et al., 2018). Mitochondria undertake fusion and fission processes all the time for maintaining the balance of bioenergetic efficiency and energy expenditure, which is involved in the pathogenesis of cerebral I/R injury (Carinci et al., 2021; Zhao et al., 2018). Currently, the mechanism of neuroprotective benefits against cerebral I/R injury by regulating mitochondrial dynamics and bioenergy is unknown. In this study, we tested the level of Mul1, Mfn2 ubiquitination, and mitochondrial dynamics and bioenergy in *in vitro* Mul1-knockdown or OGD/R-induced neuronal cells and *in vivo* I/R rat model. The major findings from this study are that cerebral I/R injury led to the imbalance of mitochondrial dynamics and a significant decrease in mitochondrial bioenergy, which is related to the binding of Mul1 to Mfn2 and its negatively regulation through ubiquitination. Furthermore, our study showed for the first time that ginsenoside CK administration could elevate fusion, reduce fission to keep the balance of mitophagy and bioenergy production by attenuating the effect of Mul1 on Mfn2 ubiquitination in cerebral I/R pathological process.

Mitochondrial fusion is a multistep and conserved process that begins with the mitofusins proteins-mediated juxtaposition and tethering of adjacent mitochondria, followed by conformational changes of mitofusins oligomers driven by GTP hydrolysis (Pernas & Scorrano, 2016). Mechanically, tethering and fusion for outer mitochondrial membrane are mainly regulated by Mfn1 and Mfn2, and homologous proteins that contain a GTPase domain (DRP1) (Ma et al., 2020). Indeed, we observed that the phenotype of I/R-induced changes in mitochondrial morphology is accompanied by a significant reduce in the expression of Mfn1, Mfn2 and OPA1, and an elevation in mitochondrial DRP1 and FIS1 expression. Importantly, we have only observed significant changes in Mfn2 levels and DRP1 translocation upon manipulation of Mul1 knockdown, leading us to consider that the Mul1-mediaed Mfn2 and DRP1 expression could drive the phenotypes in I/R injury model. Multiple studies reported that Mul1 retards mitochondrial fusion through the ubiquitination and degradation of Mfn2 in the C-terminal RING finger domain, involved in the imbalance of mitochondrial dynamics, mitophagy, and bioenergy during metabolism stress (Puri et al., 2020). Using co-IP experiment, we found that Mul1 physically interacts with Mfn2 for the degradation by ubiquitination in I/R- and OGD/R-induced neuronal injury models. The signal of Mul1-mediated removal of Mfn2 and the stabilization of DRP1 lead to extensive mitochondrial fragmentation, mitophagy and bioenergy dysfunction observed during I/R injury. Furthermore, we clearly show that knockdown of Mul1 abolished I/R-induced mitochondrial fragmentation and renovation through mitophagy and mitochondrial depolarization, suggesting that Mul1-induced mitochondrial dysfunction has a critical role in the progression of I/R injury. In addition, we found that ginsenoside CK pretreatment significantly inhibited the binding of Mul1 to Mfn2 to mediate Mfn2 degradation, thereby account for the expansive and fused network of healthy mitochondria and further prevented mitochondrial dysfunction in response to I/R and OGD/R damages. Our findings provide new insight into the potential targets during I/R injury and new molecular mechanism of ginsenoside CK, which are associated with mitochondrial dynamics and bioenergy.

Mitochondrial fragmentation-induced mitophagy and apoptosis are almost always observed during cerebral I/R injury, and DRP1 has therefore been mechanistically implicated in programmed cell apoptosis (Anzell et al., 2018; Zuo et al., 2016). Emerging evidence suggests that DRP1 stimulates Bax oligomerization and cytochrome c release by promoting mitochondrial fission and mitophagy, which are widely recognized as a culprit of neuronal injury, even programmed cell death (Yang et al., 2018; Yin et al., 2017). However, in some studies, genetic or chemical overexpression of DRP1, accompanying by strengthened mitophagy and decreased cytochrome c release, are critical neuroprotective response against neuronal I/R injury (Chen et al., 2014). Thus, there is an ongoing debate about whether the inhibition of fragmentation-induced mitophagy during cerebral I/R injury is beneficial or not (Yang et al., 2018).. In this respect, we observed that I/R- or OGD/R incubation caused the changes of mitochondrial morphology, bioenergy imbalance, and neuronal injury, which are all accompanied by the translocation of DRP1 to mitochondria. Importantly, these phenotypes above were significantly reversed by ginsenoside CK pretreatment in the cell and animal models. In addition, the targeted inhibition of DRP1 by Mdivi-1 completely abolished the restrained effect of ginsenoside CK on I/R-induced mitophagy and mito-ROS burst, but did not abrogated the interaction of Mul1 with Mfn2, which indicated that ginsenoside CK pretreatment inhibited the Mul1-regulated ubiquitination of Mfn2 to abolish DRP1-mediated fission, mitophagy and apoptosis.

Ginsenoside CK is a secondary ginsenoside biotransformed from major ginsenosides, such as Rb1, Rb2, or Rc (Park et al., 2017). Previous reports have shown that ginsenoside CK significantly inhibits I/R-induced rat neurological damage and OGD/R-induced neuronal autophagy and apoptosis (Huang et al., 2020; Park et al., 2012). Furthermore, ginsenoside CK administration can regulate multiple signal pathways related to energy metabolism, such as PI3K and AMPK in OGD/R-induced injury models (Huang et al., 2020; Li et al., 2018). Ginsenoside Rc, a metabolic precursor of ginsenoside CK, can significantly restore the imbalance of neuronal energy metabolism and mitochondrial dysfunction induced by OGD/R or I/R injury (Huang, Su, et al., 2021). Inspired by this interaction, we speculate ginsenoside CK

can regulate mitochondrial dynamics and bioenergy, thus protecting neuron from cerebral I/R injury. Therefore, when we studied the mechanism of I/R damage based on mitochondrial dynamics and bioenergetics, we carried out the screening for different ginsenoside monomers. We expectedly found a typical dose-dependent effect of ginsenoside CK on mitochondrial aspect ratio, ATP level, and OCR in OGD/R-induced neuronal injury model. More importantly, ginsenoside CK pretreatment inhibited the expression of Mul1 to regulate Mfn2 ubiquitination, mitochondrial dynamic and bioenergy, which contribute to maintain the mitochondrial integrity and neuroprotective properties in *in vivo* I/R and *in vitro* OGD/R models. These results provide a new mechanism for the beneficial effects of ginsenoside CK as natural preventive agent against cerebral I/R injury

Of note, this study still remains the limitations. First, mito-ROS was produced from complex I and complex III in cerebral I/R injury. In this study, total mito-ROS production was determined using MitoSOX™ dye, which could not specify the ROS from complex I or complex III. Particularly, accumulating evidence suggests that ROS produced by the complex I caused the neuronal deleterious effect, whereas ROS produced by complex III played the neuroprotective effect in mice with cerebral I/R injury (Chouchani et al., 2016). Future studies are needed to determine how ginsenoside CK regulates ROS production by complex I or complex III to explain the potential function of ginsenoside CK on the reduction of mito-ROS production and mitochondrial depolarization. Secondly, ginsenoside CK has been suggested to regulate the interaction of Mul1 with Mfn2; whether ginsenoside CK defined as a Mul1 inhibitor is worth further investigation. Finally, more robust data should be provided to substantiate these findings for protective effect of ginsenoside CK against cerebral injury using Mul1 loss-of-function animal models.

5 CONCLUSIONS

In conclusion, we show that I/R stimuli upregulated the binding of Mul1 to Mfn2 to regulate Mfn2 ubiquitination and degradation, which resulted in increased mitochondrial fission, bioenergy dysfunction, neuronal apoptosis, and neurological

impairment. Consistently, Mul1 suppression induced by ginsenoside CK pretreatment or knockdown exerts beneficial effect against cerebral I/R injury by abolishing mitochondrial fission, mitophagy and bioenergy dysfunction. Collectively, these data for the first time explain the molecular basis for the Mul-dependent mitochondrial dysfunctions during I/R damages and provide the evidence that ginsenoside CK may be a promising therapeutic agent against cerebral I/R injury by targeting Mul1/Mfn2-mediated mitochondrial dynamics and bioenergy.

REFERENCES

Anzell, A., Maizy, R., Przyklenk, K., & Sanderson, T. (2018). Mitochondrial Quality Control and Disease: Insights into Ischemia-Reperfusion Injury. *Molecular neurobiology*, *55*(3), 2547-2564. https://doi.org/10.1007/s12035-017-0503-9

Bederson, J., Pitts, L., Tsuji, M., Nishimura, M., Davis, R., & Bartkowski, H. (1986). Rat middle cerebral artery occlusion: evaluation of the model and development of a neurologic examination. *Stroke*, *17*(3), 472-476. https://doi.org/10.1161/01.str.17.3.472

Burté, F., Carelli, V., Chinnery, P., & Yu-Wai-Man, P. (2015). Disturbed mitochondrial dynamics and neurodegenerative disorders. *Nature reviews. Neurology*, *11*(1), 11-24. https://doi.org/10.1038/nrneurol.2014.228

Carinci, M., Vezzani, B., Patergnani, S., Ludewig, P., Lessmann, K., Magnus, T., Casetta, I., Pugliatti, M., Pinton, P., & Giorgi, C. (2021). Different Roles of Mitochondria in Cell Death and Inflammation: Focusing on Mitochondrial Quality Control in Ischemic Stroke and Reperfusion. *Biomedicines*, *9*(2). https://doi.org/10.3390/biomedicines9020169

Chandel, N. (2014). Mitochondria as signaling organelles. *BMC biology*, *12*, 34. https://doi.org/10.1186/1741-7007-12-34

Chen, W., Sun, Y., Liu, K., & Sun, X. (2014). Autophagy: a double-edged sword for neuronal survival after cerebral ischemia. *Neural regeneration research*, *9*(12), 1210-1216. https://doi.org/10.4103/1673-5374.135329

Cheng, Q., Wan, Y., Yang, W., Tian, M., Wang, Y., He, H., Zhang, W., & Liu, X. (2020). Gastrodin protects H9c2 cardiomyocytes against oxidative injury by ameliorating imbalanced mitochondrial dynamics and mitochondrial dysfunction. *Acta pharmacologica Sinica*, *41*(10), 1314-1327. https://doi.org/10.1038/s41401-020-0382-x

Chipuk, J., Mohammed, J., Gelles, J., & Chen, Y. (2021). Mechanistic connections between mitochondrial biology and regulated cell death. *Developmental cell*, *56*(9), 1221-1233. https://doi.org/10.1016/j.devcel.2021.03.033

Chouchani, E., Pell, V., James, A., Work, L., Saeb-Parsy, K., Frezza, C., Krieg, T., & Murphy, M. (2016). A Unifying Mechanism for Mitochondrial Superoxide Production during Ischemia-Reperfusion Injury. *Cell metabolism*, *23*(2), 254-263. https://doi.org/10.1016/j.cmet.2015.12.009

Gao, S., & Hu, J. (2021). Mitochondrial Fusion: The Machineries In and Out. *Trends in cell biology*, *31*(1), 62-74. https://doi.org/10.1016/j.tcb.2020.09.008

Geng, J., Liu, W., Gao, J., Jiang, C., Fan, T., Sun, Y., Qin, Z., Xu, Q., Guo, W., & Gao, J. (2019). Andrographolide alleviates Parkinsonism in MPTP-PD mice via targeting mitochondrial fission mediated by dynamin-related protein 1. *British journal of pharmacology*, *176*(23), 4574-4591. https://doi.org/10.1111/bph.14823

Gong, S., Cao, G., Li, F., Chen, Z., Pan, X., Ma, H., Zhang, Y., Yu, B., & Kou, J. (2021). Endothelial Conditional Knockdown of NMMHC IIA (Nonmuscle Myosin Heavy Chain IIA) Attenuates Blood-Brain Barrier Damage During Ischemia-Reperfusion Injury. *Stroke*, *52*(3), 1053-1064. https://doi.org/10.1161/strokeaha.120.031410

Guo, S., Zhang, Y., Peng, J., Li, Y., Liu, W., Tang, M., Zhang, X., Yang, J., Peng, J., & Luo, X. (2019). Natural compound methyl protodioscin protects rat brain from ischemia/reperfusion injury through regulation of Mul1/SOD2 pathway. *European journal of pharmacology*, *849*, 50-58. https://doi.org/10.1016/j.ejphar.2019.01.057

Han, J., Li, Q., Ma, Z., & Fan, J. (2017). Effects and mechanisms of compound Chinese medicine and major ingredients on microcirculatory dysfunction and organ injury induced by ischemia/reperfusion. *Pharmacology & therapeutics*, *177*, 146-173. https://doi.org/10.1016/j.pharmthera.2017.03.005

Huang, Q., Gao, S., Zhao, D., & Li, X. (2021). Review of ginsenosides targeting mitochondrial function to treat multiple disorders: Current status and perspectives. *Journal of ginseng research*, *45*(3), 371-379. https://doi.org/10.1016/j.jgr.2020.12.004

Huang, Q., Lou, T., Wang, M., Xue, L., Lu, J., Zhang, H., Zhang, Z., Wang, H., Jing, C., Zhao, D., Sun, L., & Li, X. (2020). Compound K inhibits autophagy-mediated apoptosis induced by oxygen and glucose deprivation/reperfusion via regulating AMPK-mTOR pathway in neurons. *Life sciences*, *254*, 117793. https://doi.org/10.1016/j.lfs.2020.117793

Huang, Q., Su, H., Qi, B., Wang, Y., Yan, K., Wang, X., Li, X., & Zhao, D. (2021). A SIRT1 Activator, Ginsenoside Rc, Promotes Energy Metabolism in Cardiomyocytes and Neurons. *Journal of the American Chemical Society*, *143*(3), 1416-1427. https://doi.org/10.1021/jacs.0c10836

Igarashi, R., Yamashita, S., Yamashita, T., Inoue, K., Fukuda, T., Fukuchi, T., & Kanki, T. (2020). Gemcitabine induces Parkin-independent mitophagy through mitochondrial-resident E3 ligase MUL1-mediated stabilization of PINK1. *Scientific reports*, *10*(1), 1465. https://doi.org/10.1038/s41598-020-58315-w

Iwata, R., Casimir, P., & Vanderhaeghen, P. (2020). Mitochondrial dynamics in postmitotic cells regulate neurogenesis. *Science (New York, N.Y.)*, *369*(6505), 858-862. https://doi.org/10.1126/science.aba9760

Kalogeris, T., Bao, Y., & Korthuis, R. (2014). Mitochondrial reactive oxygen species: a double edged sword in ischemia/reperfusion vs preconditioning. *Redox biology*, *2*, 702-714. https://doi.org/10.1016/j.redox.2014.05.006

Kim, H., Kim, T., Kang, L., Kim, Y., Kang, M., Kim, J., Ryu, J., Hyeon, T., Yoon, B., Ko, S., & Kim, B. (2020). Mesenchymal stem cell-derived magnetic extracellular nanovesicles for targeting and treatment of ischemic stroke. *Biomaterials*, *243*, 119942. https://doi.org/10.1016/j.biomaterials.2020.119942

Kumar, R., Bukowski, M., Wider, J., Reynolds, C., Calo, L., Lepore, B., Tousignant, R., Jones, M., Przyklenk, K., & Sanderson, T. (2016). Mitochondrial dynamics following global cerebral ischemia. *Molecular and cellular neurosciences*, *76*, 68-75. https://doi.org/10.1016/j.mcn.2016.08.010

Li, X., Huang, Q., Wang, M., Yan, X., Song, X., Ma, R., Jiang, R., Zhao, D., & Sun, L. (2018). Compound K Inhibits Autophagy-Mediated Apoptosis Through Activation of the PI3K-Akt Signaling Pathway Thus Protecting Against Ischemia/Reperfusion Injury. *Cellular physiology and biochemistry : international journal of experimental cellular physiology, biochemistry, and pharmacology*, *47*(6), 2589-2601. https://doi.org/10.1159/000491655

Lilley, E., Stanford, S., Kendall, D., Alexander, S., Cirino, G., Docherty, J., George, C., Insel, P., Izzo, A., Ji, Y., Panettieri, R., Sobey, C., Stefanska, B., Stephens, G., Teixeira, M., & Ahluwalia, A. (2020). ARRIVE 2.0 and the British Journal of Pharmacology: Updated guidance for 2020. *British journal of pharmacology*, *177*(16), 3611-3616. https://doi.org/10.1111/bph.15178

Liu, F., Lu, J., Manaenko, A., Tang, J., & Hu, Q. (2018). Mitochondria in Ischemic Stroke: New Insight and Implications. *Aging and disease*, *9*(5), 924-937. https://doi.org/10.14336/ad.2017.1126

Liu, Q., & Dong, Q. (2020). NR4A2 Exacerbates Cerebral Ischemic Brain Injury via Modulating microRNA-652/Mul1 Pathway. *Neuropsychiatric disease and treatment*, *16*, 2285-2296. https://doi.org/10.2147/ndt.s265601

Longa, E., Weinstein, P., Carlson, S., & Cummins, R. (1989). Reversible middle cerebral artery occlusion without craniectomy in rats. *Stroke*, *20*(1), 84-91. https://doi.org/10.1161/01.str.20.1.84

Ma, R., Ma, L., Weng, W., Wang, Y., Liu, H., Guo, R., Gao, Y., Tu, J., Xu, T., Cheng, J., Zhu, M., Zhou, A., & Li, Y. (2020). DUSP6 SUMOylation protects cells from oxidative damage via direct regulation of Drp1 dephosphorylation. *Science advances*, *6*(13), eaaz0361. https://doi.org/10.1126/sciadv.aaz0361

Oh, J., Jeong, J., Park, S., & Chun, S. (2020). Ginsenoside Compound K Induces Adult Hippocampal Proliferation and Survival of Newly Generated Cells in Young and Elderly Mice. *Biomolecules*, *10*(3). https://doi.org/10.3390/biom10030484

Oh, J., & Kim, J. (2016). Compound K derived from ginseng: neuroprotection and cognitive improvement. *Food & function*, *7*(11), 4506-4515. https://doi.org/10.1039/c6fo01077f

Park, J., Shin, J., Jung, J., Hyun, J., Van Le, T., Kim, D., Park, E., & Kim, H. (2012). Anti-inflammatory mechanism of compound K in activated microglia and its neuroprotective effect on experimental stroke in mice. *The Journal of pharmacology and experimental therapeutics*, *341*(1), 59-67. https://doi.org/10.1124/jpet.111.189035

Park, S., Na, C., Yoo, S., Seo, S., & Son, H. (2017). Biotransformation of major ginsenosides in ginsenoside model culture by lactic acid bacteria. *Journal of ginseng research*, *41*(1), 36-42. https://doi.org/10.1016/j.jgr.2015.12.008

Pernas, L., & Scorrano, L. (2016). Mito-Morphosis: Mitochondrial Fusion, Fission, and Cristae Remodeling as Key Mediators of Cellular Function. *Annual review of physiology*, *78*, 505-531. https://doi.org/10.1146/annurev-physiol-021115-105011

Puri, R., Cheng, X., Lin, M., Huang, N., & Sheng, Z. (2019). Mul1 restrains Parkin-mediated mitophagy in mature neurons by maintaining ER-mitochondrial contacts. *Nature communications*, *10*(1), 3645. https://doi.org/10.1038/s41467-019-11636-5

Puri, R., Cheng, X., Lin, M., Huang, N., & Sheng, Z. (2020). Defending stressed mitochondria: uncovering the role of MUL1 in suppressing neuronal mitophagy. *Autophagy*, *16*(1), 176-178. https://doi.org/10.1080/15548627.2019.1687216

Raimundo, L., Paterna, A., Calheiros, J., Ribeiro, J., Cardoso, D., Piga, I., Neto, S., Hegan, D., Glazer,

P., Indraccolo, S., Mulhovo, S., Costa, J., Ferreira, M., & Saraiva, L. (2021). BBIT20 inhibits homologous DNA repair with disruption of the BRCA1-BARD1 interaction in breast and ovarian cancer. *British journal of pharmacology*. https://doi.org/10.1111/bph.15506

Schmitt, K., Grimm, A., Dallmann, R., Oettinghaus, B., Restelli, L., Witzig, M., Ishihara, N., Mihara, K., Ripperger, J., Albrecht, U., Frank, S., Brown, S., & Eckert, A. (2018). Circadian Control of DRP1 Activity Regulates Mitochondrial Dynamics and Bioenergetics. *Cell metabolism*, *27*(3), 657-666.e655. https://doi.org/10.1016/j.cmet.2018.01.011

Sharma, A., & Lee, H. (2020). Ginsenoside Compound K: Insights into Recent Studies on Pharmacokinetics and Health-Promoting Activities. *Biomolecules*, *10*(7). https://doi.org/10.3390/biom10071028

Ten, V., & Galkin, A. (2019). Mechanism of mitochondrial complex I damage in brain ischemia/reperfusion injury. A hypothesis. *Molecular and cellular neurosciences*, *100*, 103408. https://doi.org/10.1016/j.mcn.2019.103408

Yang, J., Mukda, S., & Chen, S. (2018). Diverse roles of mitochondria in ischemic stroke. *Redox biology*, *16*, 263-275. https://doi.org/10.1016/j.redox.2018.03.002

Yin, Y., Sun, G., Li, E., Kiselyov, K., & Sun, D. (2017). ER stress and impaired autophagy flux in neuronal degeneration and brain injury. *Ageing research reviews*, *34*, 3-14. https://doi.org/10.1016/j.arr.2016.08.008

Yu, H., Guan, Q., Guo, L., Zhang, H., Pang, X., Cheng, Y., Zhang, X., & Sun, Y. (2016). Gypenosides alleviate myocardial ischemia-reperfusion injury via attenuation of oxidative stress and preservation of mitochondrial function in rat heart. *Cell stress & chaperones*, *21*(3), 429-437. https://doi.org/10.1007/s12192-016-0669-5

Yuan, Y., Li, X., Xu, Y., Zhao, H., Su, Z., Lai, D., Yang, W., Chen, S., He, Y., Li, X., Liu, L., & Xu, G. (2019). Mitochondrial E3 ubiquitin ligase 1 promotes autophagy flux to suppress the development of clear cell renal cell carcinomas. *Cancer science*, *110*(11), 3533-3542. https://doi.org/10.1111/cas.14192

Zhang, Q., Wang, Z., Miao, L., Wang, Y., Chang, L., Guo, W., & Zhu, Y. (2019). Neuroprotective Effect of SCM-198 through Stabilizing Endothelial Cell Function. *Oxidative medicine and cellular longevity*, *2019*, 7850154. https://doi.org/10.1155/2019/7850154

Zhao, H., Pan, W., Chen, L., Luo, Y., & Xu, R. (2018). Nur77 promotes cerebral ischemia-reperfusion injury via activating INF2-mediated mitochondrial fragmentation. *Journal of molecular histology*, *49*(6), 599-613. https://doi.org/10.1007/s10735-018-9798-8

Zuo, W., Yang, P., Chen, J., Zhang, Z., & Chen, N. (2016). Drp-1, a potential therapeutic target for brain ischaemic stroke. *British journal of pharmacology*, *173*(10), 1665-1677. https://doi.org/10.1111/bph.13468

Figures and figure legends

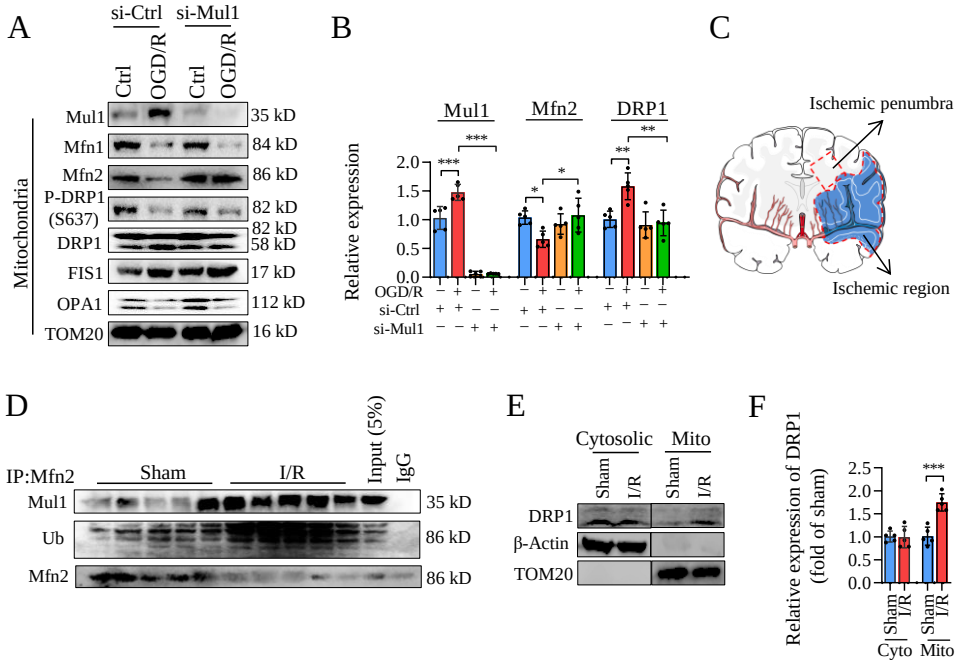

Figure 1. Mul1 ubiquitinated and targeted Mfn2 in OGD/R and I/R injury models. (A) After PC12 cells transfected with si-Mul1 or si-Ctrl siRNAs, the expression of protein-related to mitochondrial fusion and fission was detected by western blot analysis. TOM20 is a loading control for mitochondrial proteins. **(B)** The densitometric analysis of Mul1, Mfn2 and DRP1 from (A); data are presented as the mean ± SD; n = 5 per group; **P* < 0.05, **P* < 0.01, and ****P* < 0.001, significantly different as indicated (one-way ANOVA followed by Tukey's post hoc test). **(C)** Illustration of the location of ischemic penumbra tissue used in the following western blot analysis for the brains of rat models. **(D)** After immunoprecipitation of Mfn2 in the proteins from fresh brain tissues (n = 5 of each group), the binding of Mfn2 to Mul1 and its ubiquitination level were determined by western blot analysis. Sham: sham operation group; I/R: ischemia/reperfusion. 5% of the lysed proteins in the co-IP experiment were used as input control (Input). **(E)** DRP1 protein expression in cytoplasm and mitochondria in the brains of rats from sham and I/R groups was analyzed by western blot; n = 5 per group; β-Actin and TOM20 is the loading control for cytosolic and mitochondrial proteins, respectively. Cytosolic: cytosolic proteins; Mito: mitochondrial proteins. **(F)** The protein expression of DRP1 was quantitatively analyzed from (E); data are shown as mean ± SEM (n = 5 of each group); ****P* < 0.001; significantly different as indicated (two-tailed Student's t-test).

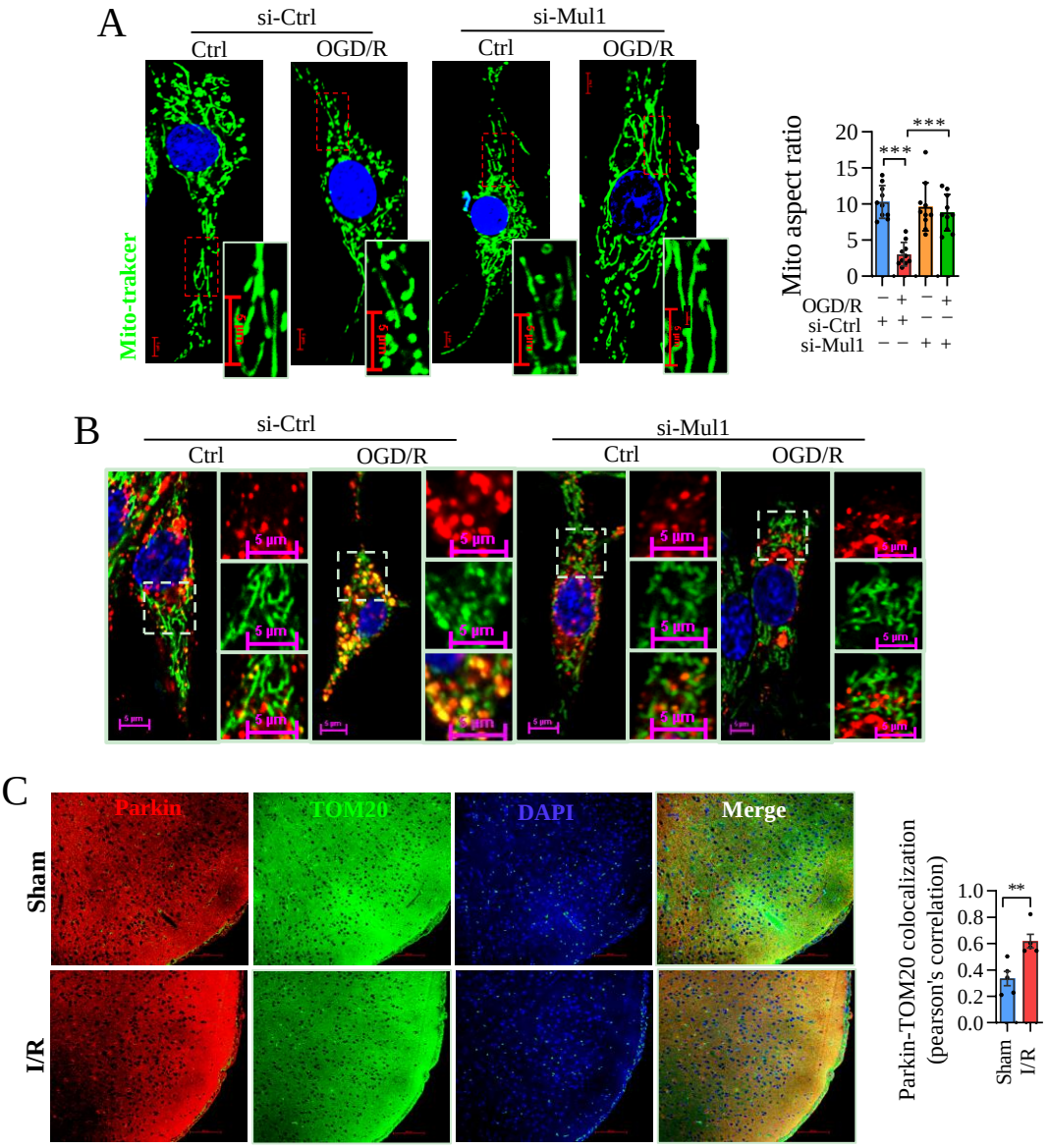

Figure 2. Mul1 is required for OGD/R-induced neuronal injury with abnormal mitochondrial dynamics and mitophagy. (A) After labeling with a Mito-Tracer fluorescent probe, the morphology of mitochondria was observed and analyzed by confocal microscope in PC12 cells with transfected with si-Ctrl or si-Mul siRNAs, prior to OGD/R incubation. The ratio of mitochondrial aspect in different groups are shown on the right; scale bar = 20 μm; data are shown as mean ± SD; n = 10 per group; ***P < 0.001, significantly different as indicated (one-way ANOVA followed by Tukey's post hoc test). **(B)** After transfected with si-Mul1 or si-Ctrl siRNAs, the mitophagy level in PC12 cells with OGD/R injury was observed by fluorescence labeling for mitochondria and lysosomes; n = 5 per group; scale bar = 20 μm. **(C)** The expression of Parkin and TOM20 in rat cortical neurons were detected by confocal microscope and the Parkin/TOM20 co-localization was analyzed using the Pearson correlation method, data are shown as mean ± SEM; n = 5 per group; ***P < 0.001, significantly different as indicated (two-tailed Student's t-test). OGD/R: oxygen glucose deprivation (2 h)/reperfusion (12 h).

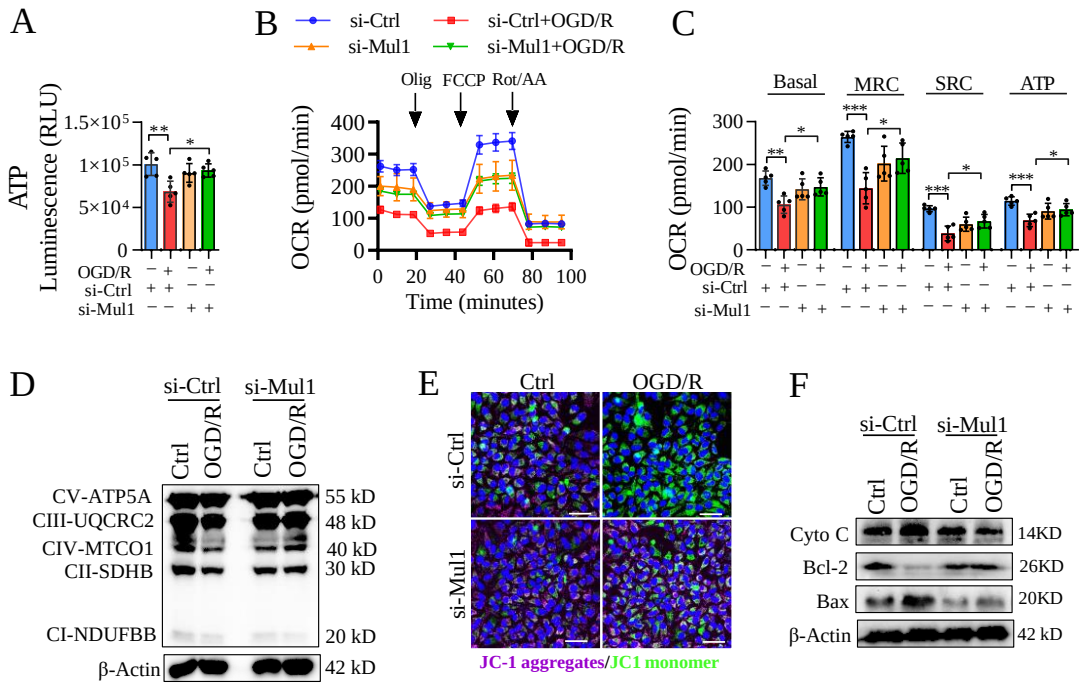

Figure 3. Mul1 is required for OGD/R-induced neuronal metabolic reprogramming and injury. (A) After transfected with si-Mul1 or si-Ctrl siRNAs ATP production in the OGD/R-induced PC12 cells was detected by bioluminescence assay; data are presented as the mean ± SD; n = 5 per group; **P* < 0.05, ***P* < 0.01, significantly different as indicated (one-way ANOVA followed by Tukey's post hoc test). **(B)** After transfected with si-Ctrl or si-Mul1 and incubated with OGD/R, PC12 cells were sequentially treated with oligomycin (Olig 1 mM), FCCP (2 mM), and rotenone (Rot, 1 mM) plus antimycin A (AA, 1 mM) to determine OCR for mitochondrial pressure assay; (n = 5 of each group). **(C)** Quantitative analysis of oxygen consumption from (B); Basal: Basal respiration; MRC: maximal respiration consumption; SPC: spare capacity; ATP: ATP-linked respiration; data are shown as mean ± SD, n = 5 per group; **P* < 0.05, ***P* < 0.01 and ****P* < 0.001, significantly different as indicated (one-way ANOVA followed by Tukey's post hoc test). **(D)** After transfected with si-Mul1 or si-Ctrl siRNAs prior to OGD/R incubation, the levels of mitochondrial complex I-V were detected by western blot (n = 5 of each group); β-Actin is a loading control. **(E)** The mitochondrial membrane potential of PC12 cells transfected with si-Mul1 or si-Ctrl siRNAs and then exposed with OGD/R damage was evaluated by the ratio of JC-1 aggregates and JC-1 monomers staining; n = 8 per group. **(F)** After OGD/R incubation, the expressions of mitochondrial apoptosis-related proteins, Cyto C, Bcl-2, and Bax in PC12 cells with si-Ctrl or si-Mul1 transfections were detected by western blot (n = 5 of each group); β-Actin is a loading control.

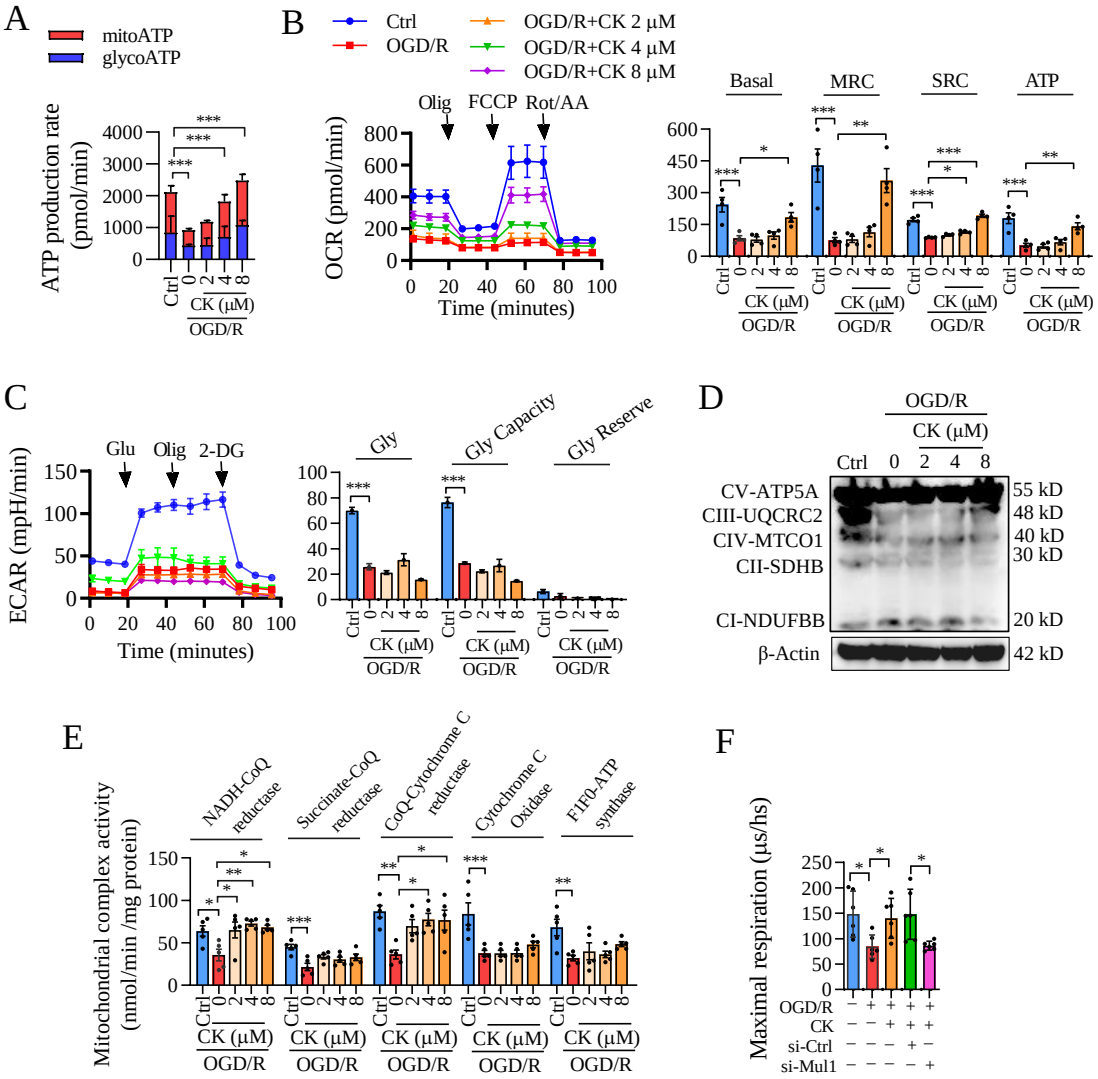

Figure 4. The effect of ginsenoside CK against neuronal bioenergy imbalance is driven by the Mul1 activity in OGD/R injury model. (A) After treatment with ginsenoside CK (2, 4 or 8 μM) for 48 h or OGD/R incubation, PC12 cells were treated with Olig or Rot plus AA to detect the ATP production originated from the mitochondria (mitoATP) or glycolysis (glycoATP); data are shown as mean ± SD; n = 5 per group; ***P < 0.001, significantly different as indicated (one-way ANOVA followed by Tukey's post hoc test). **(B)** Oxygen consumption of PC12 cells pretreated with ginsenoside CK for 48 h and exposed with OGD/R injury was measured and analyzed by Seahorse XFe24 multifunctional energy metabolizer and mitochondrial pressure kit; The relative levels of oxygen consumption for basal respiration (Basal), maximal respiration consumption (MRC), spare capacity (SPC), and ATP-linked respiration (ATP) are shown on right. data are shown as mean ± SD, n = 5 per group ; *P < 0.05, **P < 0.01 and ***P < 0.001, significantly different as indicated (one-way ANOVA followed by Tukey's post hoc test). **(C)** Glycolysis (Gly), glycolytic capacity (Gly Capacity), and glycolytic reserve (Gly Reserve) in PC12 cells pretreated with ginsenoside CK for 48 h prior to OGD/R incubation were determined by the sequential addition of 10 mM glucose (Glu), 1 μM oligomycin (Olig), or 50

mM 2-deoxy-D-glucose (2-DG) using measuring extracellular acidification rate (ECAR); data are shown as mean ± SD, n = 5 per group; ***$P < 0.001$, significantly different as indicated (one-way ANOVA followed by Tukey's post hoc test). **(D)** After pretreatment with ginsenoside CK (2, 4 or 8 μM) for 48 h, prior to OGD/R incubation, the expression of mitochondrial complex protein I-V in PC12 cells was detected by western blot (n=5 of each group). β-Actin is a loading control. **(E)** The activities of five mitochondrial electron transfer chain enzymes in OGD/R-induced PC12 cells untreated and treated with ginsenoside CK for 48 h were determined by enzymatic reaction kinetics kit; data are shown as mean ± SD, n = 5 per group; *$P < 0.05$, **$P < 0.01$ and ***$P < 0.001$, significantly different as indicated (one-way ANOVA followed by Tukey's post hoc test). **(F)** The maximal oxygen consumption was analyzed by LUXCEL oxygen consumption probe in the PC12 cells transfected with si-Ctrl, si-Mul and/or pretreated with ginsenoside CK; data are shown as mean ± SD, n = 5 per group; *$P < 0.05$, significantly different as indicated (one-way ANOVA followed by Tukey's post hoc test).

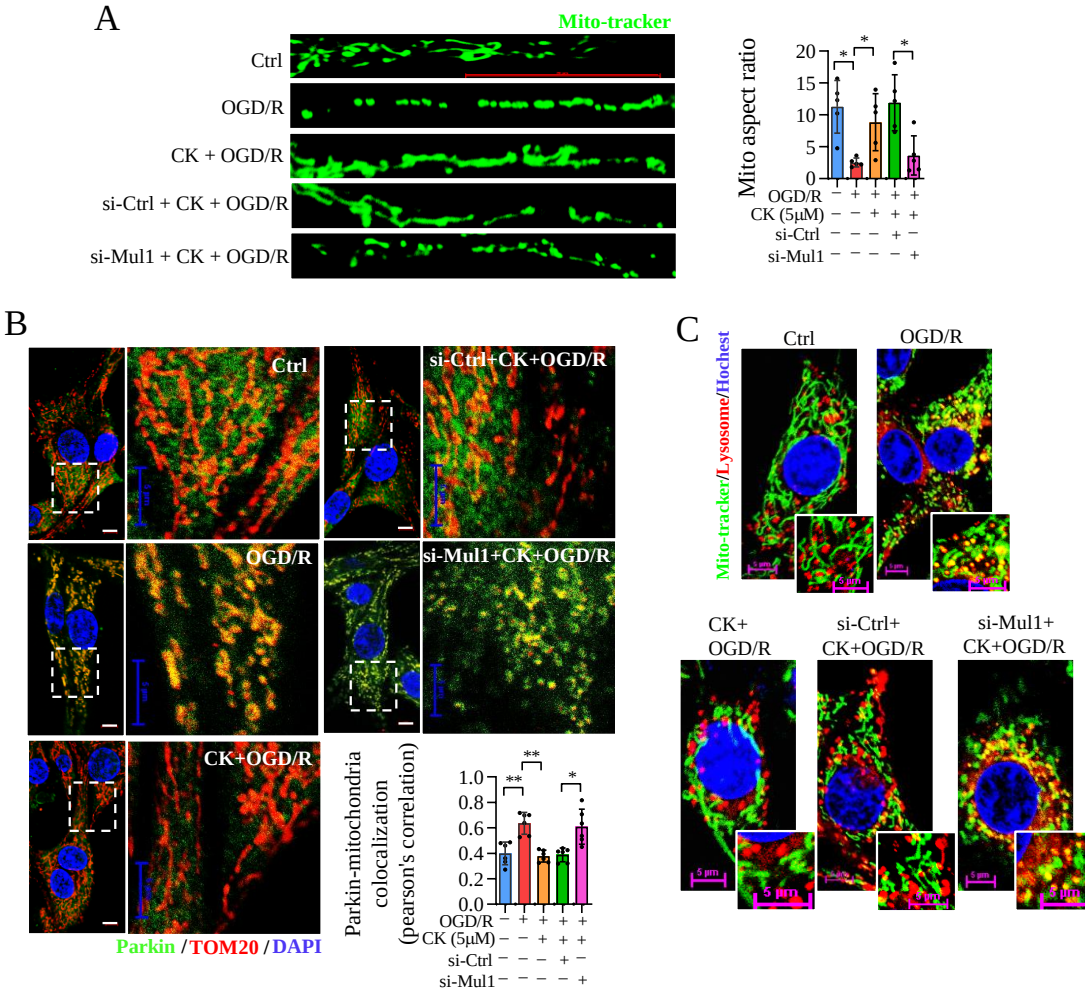

Figure 5. Ginsenoside CK augmented mitochondrial fusion and inhibited mitophagy through Mul1 in OGD/R-induced PC12 injury model. (A) After labeling with Mito-tracker probe, mitochondria morphology was visualized to analyze mitochondria aspect ratio in OGD/R-induced PC12 cells pretreated with ginsenoside CK for 48 h, and transfected with si-Ctrl or si-Mul1 siRNAs; scale bar = 20 μm; data are shown as mean ± SD, n = 5 per group; **P* < 0.05, significantly different as indicated (one-way ANOVA followed by Tukey's post hoc test). **(B)** After pretreatment with 4 μM ginsenoside CK for 48 h prior to OGD/R incubation, the co-localization of Parkin and TOM20 was detected and analyzed in PC12 cells transfected with si-Ctrl or si-Mul1; DAPI is used for staining nucleus. scale bar = 5 μm; data are shown as mean ± SD; n = 5 per group; **P* < 0.05, ***P* < 0.01; significantly different as indicated (one-way ANOVA followed by Tukey's post hoc test). **(C)** After transfection with si-Ctrl or si-Mul1 siRNAs and ginsenoside CK pretreatment, the co-location of mitochondria and lysosomes was visualized in OGD/R-induced PC12 cells by confocal microscope; Hochest 33254 is used for nuclear staining; n = 5 per group; scale bar = 5 μm.

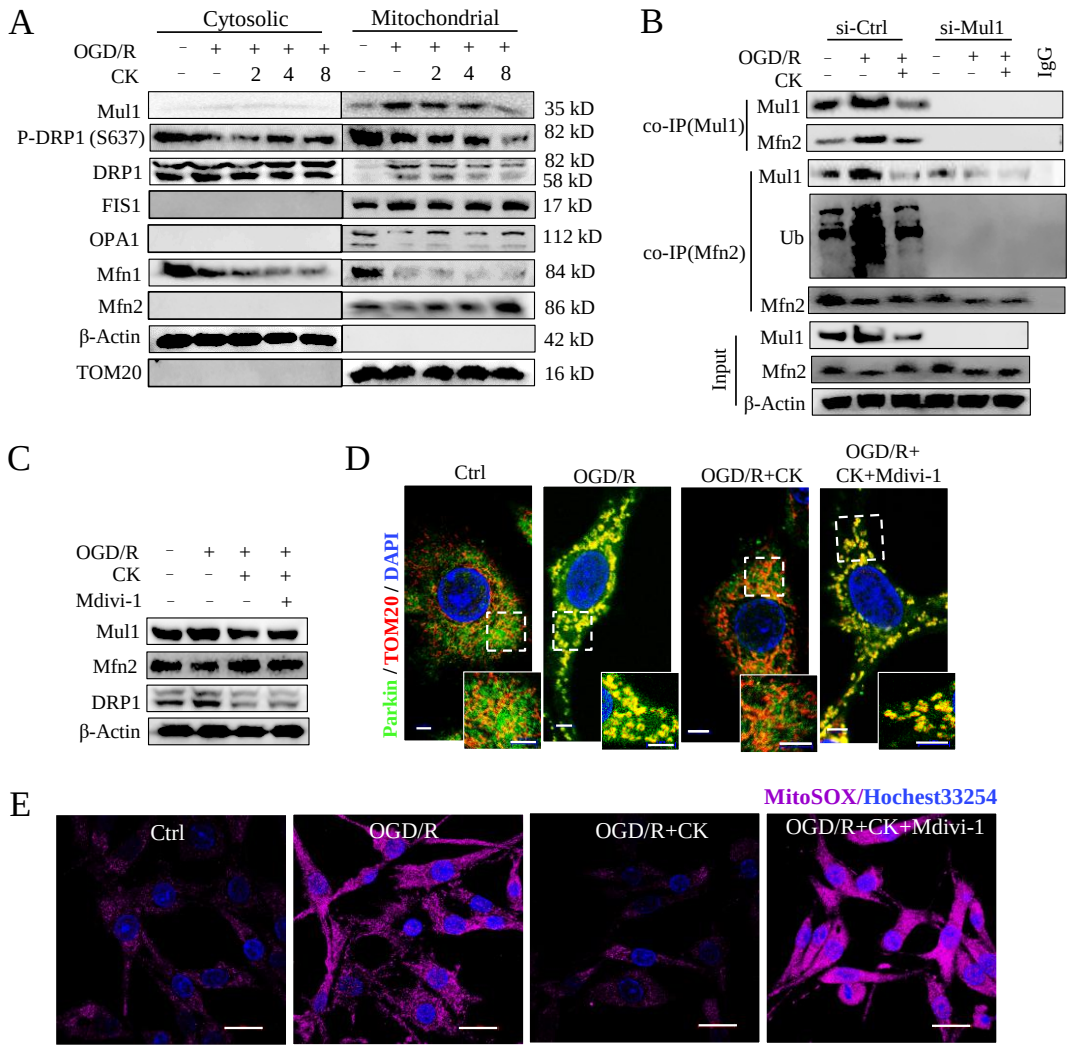

Figure 6. Ginsenoside CK inhibits mitochondrial dynamic imbalance and damage by inhibiting the ubiquitination of Mfn2 by Mul1. (A) After 2, 4, or 8 μM ginsenoside CK pretreatment, prior to OGD/R incubation, the expression of Mul1 and mitochondrial dynamic-related proteins in cytoplasm or mitochondria was detected by western blot (n = 5 of each group); β-Actin and TOM20 is the loading control for cytosolic and mitochondrial proteins, respectively. **(B)** After Mul1 or Mfn2 were immunoprecipitated, the binding and ubiquitination level of Mfn2 in mitochondrial proteins from OGD/R-induced PC12 cells transfected with si-Ctrl or si-Mul1 siRNAs, and pretreated with ginsenoside CK for 48 h were detected by western blot analysis (n = 5 of each group). 10% of the lysed mitochondrial proteins in the co-IP experiment were used as input control. **(C)** After pretreatment with ginsenoside CK or Mdivi-1 for 48 h prior to OGD/R incubation, the expression of Mul1, Mfn2, and DRP1 were detected by western blot (n = 5 of each group); β-Actin is a loading control. **(D)** The co-expression of Parkin and TOM20 was detected after pretreatment with 4 μM ginsenoside CK or Mdivi-1, prior to OGD/R incubation; n = 5 per group; scale bar = 5 μm. **(E)** The level of mitochondrial ROS (MitoSox) in PC12 cells was determined by confocal microscope; n = 5 per group; scale bar = 20 μm. Hochest 33254 is a nuclear counterstain.

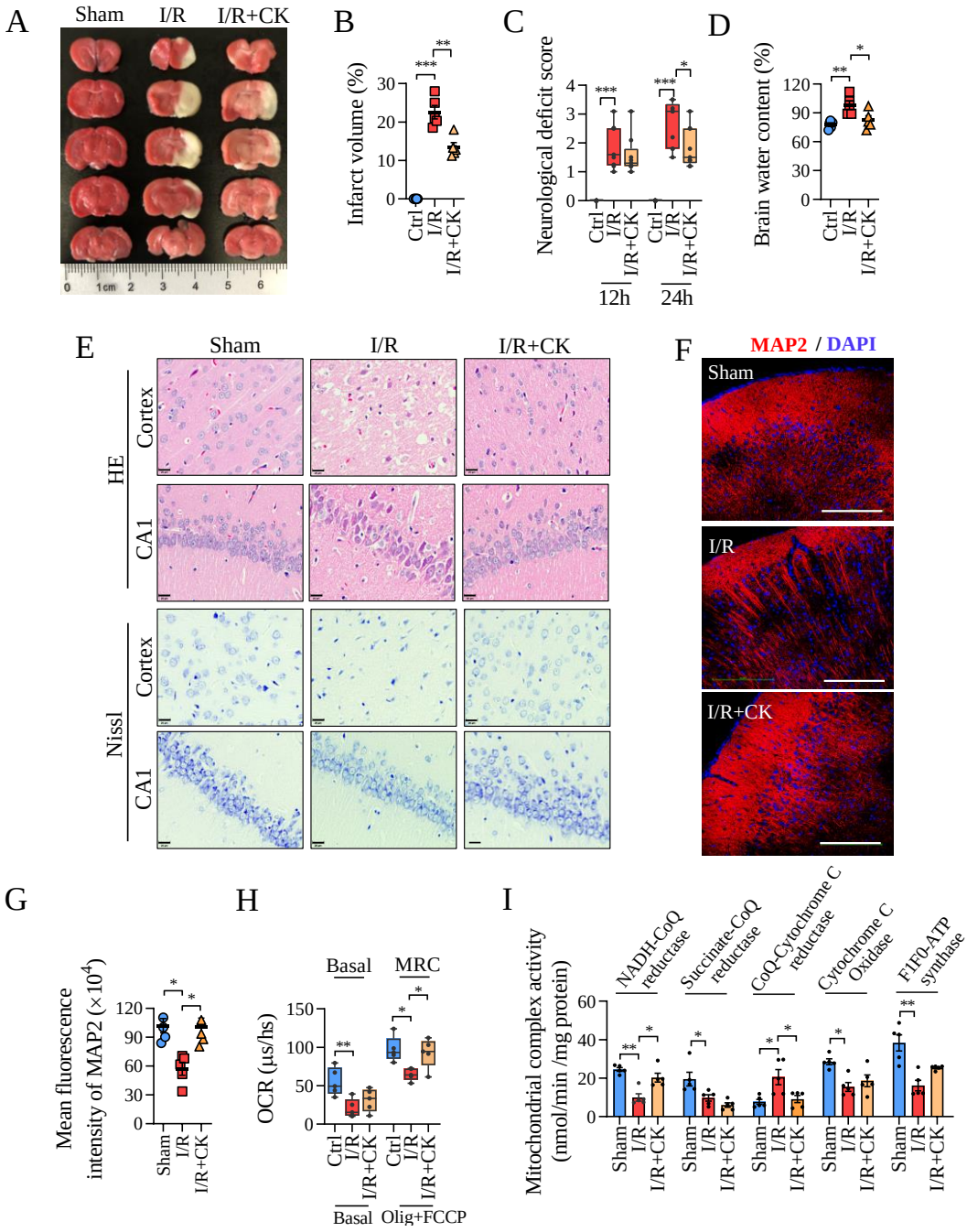

Figure 7. Ginsenoside CK reduces neuronal injury and mitochondrial damage in I/R rat model. (A) After ginsenoside CK pretreatment (10 mg/kg/day, 500μl, dissolved in ddH_2O) for 14 days prior to I/R injury, TTC staining was used to detect the ischemic area in rat brain tissues from Sham group without insert the nylon monofilament, n = 5), I/R group (middle cerebral artery occlusion, n = 5), and I/R+CK group (n = 5); the red represents the living neurons, and the white represents the damaged neurons. **(B)** The ischemic volume in rat brain tissues from (A) was analyzed by Image J software; data are shown as mean ± SEM, n = 5 per group; $^{**}P < 0.01$, $^{***}P < 0.001$, significantly different as indicated (one-way ANOVA followed by Tukey's post hoc test). **(C)** Longa neurological deficiency scale was used to analyze the neurological function of rats from Sham, I/R, and I/R+CK groups, after

I/R injury at 12 h or 24 h; data are shown as mean ± SEM, n = 5 per group; *$P < 0.05$, ***$P < 0.001$, significantly different as indicated (one-way ANOVA followed by Tukey's post hoc test). **(D)** The water content of brain tissue was measured by dry and wet weight method; data are expressed as mean ± SEM, n = 5 per group; *$P < 0.05$ and **$P < 0.01$, significantly different as indicated (one-way ANOVA followed by Tukey's post hoc test). **(E)** After ginsenoside CK pretreatment and I/R injury, H&E and Nissl staining were used to analyze the degree of neuronal damage in cerebral cortex and CA1 regions of rat brains (n = 5 of each group); scale bar = 20 μm. **(F)** The expression of MAP2 in cerebral cortex was detected by immunofluorescence assay; DAPI is used for staining nuclei (n = 5 of each group); scale bar = 200 μm. **(G)** Quantitative analysis of the mean fluorescence intensity of, MAP2 in rat brain tissues from (F) in the Sham, I/R, and I/R+CK groups; data are shown as mean ± SEM, n = 5 per group; *$P < 0.05$, significantly different as indicated (one-way ANOVA followed by Tukey's post hoc test). **(H)** Live mitochondria from cerebral cortical neurons of different groups were extracted to measure OCR in basal respiration and under the mitochondrial stress with oligomycin and FCCP using the LUXCEL oxygen consumption kit; data are shown as mean ± SEM, n = 5 per group; *$P < 0.05$, **$P < 0.01$, significantly different as indicated; one-way ANOVA followed by Tukey's post hoc test. **(I)** Enzyme activity of the five mitochondrial complexes in cerebral cortical neurons of rat brain tissues from Sham, I/R, and I/R+CK groups was were examined by enzymatic kits; data are shown as mean ± SEM, n = 5 per group; *$P < 0.05$, **$P < 0.01$, significantly different as indicated (one-way ANOVA followed by Tukey's post hoc test).

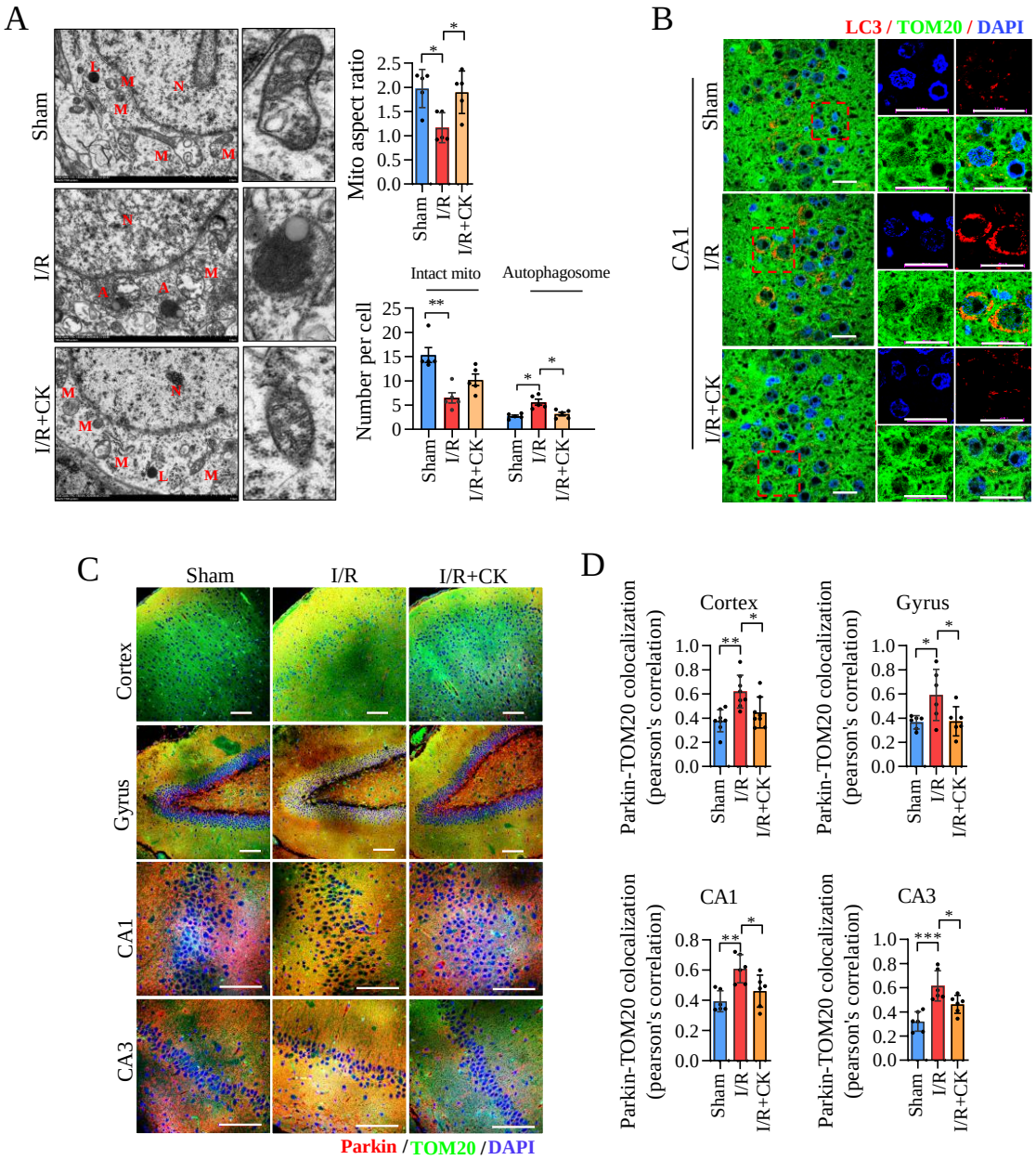

Figure 8. Ginsenoside CK reduced mitochondrial fragmentation and mitophagy in I/R model. (A) The ultrastructural morphology of mitochondria in rat brain tissues from Sham, I/R, and I/R+CK groups was examined by transmission electron microscopy. A: autophagosome, L: lysosome, M: mitochondria. N: nucleus. The aspect ratio of mitochondria and the numbers of mitochondrial autophagy lysosomes were statistically analyzed and are shown on right; scale bar = 1 μm, data are shown as mean ± SEM, n = 5 per group; **P* < 0.05 and ***P* < 0.01, significantly different as indicated (one-way ANOVA followed by Tukey's post hoc test). **(B)** The expression and localization of LC3 and TOM20 in neurons of CA1 region from rats with Sham, I/R, and I/R+CK groups were detected by immunofluorescence assay; n = 5 per group; DAPI is used for staining nuclei; scale bar = 200 μm. **(C)** The expression and localization of Parkin and TOM20 in neurons of different regions, including cortex, gyrus, CA1 or CA3 of rats from Sham group (n = 5), I/R group (n = 5), and I/R+CK

group (n = 5) were detected by immunofluorescence assay. DAPI is used for staining nuclei; scale bar = 200 μm. **(D)** The co-localization of Parkin and TOM20 in neurons of different regions from (C) was quantitatively analyzed; data are shown as mean ± SEM; n = 6 per group; **P* < 0.05, ***P* < 0.01, ****P* < 0.001, significantly different as indicated; one-way ANOVA followed by Tukey's post hoc test.

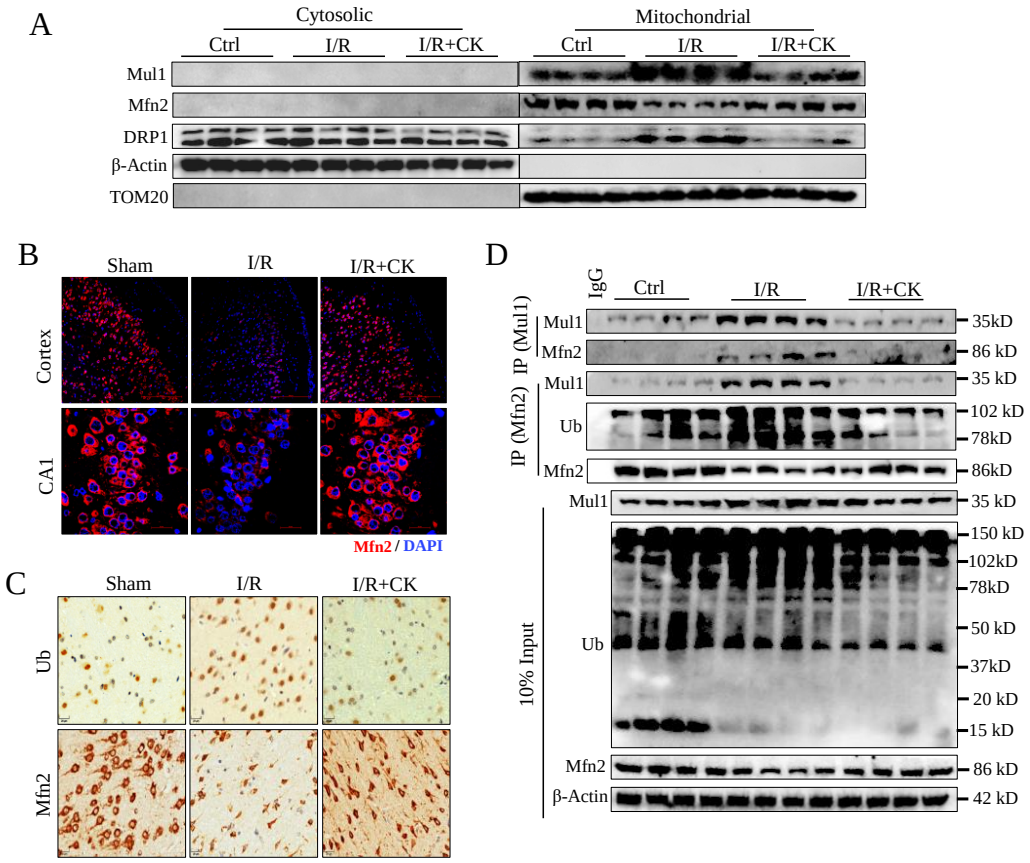

Figure 9. Ginsenoside CK inhibits the activity of Mul1 and ubiquitination of Mfn2 in I/ R rat model. (A) After ginsenoside CK administration for 14 days and I/R injury, the protein expressions of Mul1, Mfn2 and DRP1 in the cytoplasm or mitochondria in rat brain tissues from Sham, I/R, and I/R+CK groups were detected by western blot; n = 5 per group; β-Actin and TOM20 is a loading control for cytosolic and mitochondrial protein. **(B)** The expression of Mfn2 protein in cortex and CA1 region were detected by immunofluorescence assay; DAPI is used for staining nuclei; scale bar = 200 μm; n = 5 per group. **(C)** The expressions of ubiquitin protein and Mfn2 protein in brain tissues from Sham, I/R, and I/R+CK groups were detected by immunohistochemical staing; n = 5 per group, scale bar = 200 μm. **(D)** After the immunoprecipitation of Mul1 or Mfn2 antibody, the binding of Mul1 and Mfn2 and Mfn2 ubiquitination in fresh brain tissues of Sham, I/R, and I/R+CK groups were analyzed by co-IP and western blot; n = 5 per group, 10% of the lysed tissue proteins in the co-IP experiment were used as input control. Ub: ubiquitination.